

AD-A208 381

ZPIMP: A Zero-D Z-Pinch Implosion Code

JOHN L. GIULIANI AND JOHN ROGERSON

*Plasma Radiation Branch
Plasma Physics Division*

April 25, 1989

This research was sponsored by the Defense Nuclear Agency under Subtask Code and Title: RL RA/Advanced Simulation Concepts, Work Unit Code and Title, 00050, X-Ray Source Development Theory.

Approved for public release; distribution unlimited.

| REPORT DOCUMENTATION PAGE | | | | Form Approved OMB No 0704-0188 | |
|---|-------|--|---|--|-------------------------------------|
| 1a REPORT SECURITY CLASSIFICATION UNCLASSIFIED | | | 1b RESTRICTIVE MARKINGS | | |
| 2a SECURITY CLASSIFICATION AUTHORITY | | | 3 DISTRIBUTION/AVAILABILITY OF REPORT Approved for public release; distribution unlimited. | | |
| 2b DECLASSIFICATION/DOWNGRADING SCHEDULE | | | | | |
| 4 PERFORMING ORGANIZATION REPORT NUMBER(S) NRL Memorandum Report 6448 | | | 5 MONITORING ORGANIZATION REPORT NUMBER(S) | | |
| 6a NAME OF PERFORMING ORGANIZATION Naval Research Laboratory | | 6b OFFICE SYMBOL (If applicable) Code 4720 | 7a NAME OF MONITORING ORGANIZATION | | |
| 6c ADDRESS (City, State, and ZIP Code) Washington, DC 20375-5000 | | | 7b ADDRESS (City, State, and ZIP Code) | | |
| 8a NAME OF FUNDING/SPONSORING ORGANIZATION Defense Nuclear Agency | | 8b OFFICE SYMBOL (If applicable) RAEV | 9 PROCUREMENT INSTRUMENT IDENTIFICATION NUMBER | | |
| 8c ADDRESS (City, State, and ZIP Code) Alexandria, VA 22310 | | | 10 SOURCE OF FUNDING NUMBERS | | |
| | | | PROGRAM ELEMENT NO 62715H | PROJECT NO RL | TASK NO RA |
| | | | | | WORK UNIT ACCESSION NO DN880-191 |
| 11 TITLE (Include Security Classification) ZPIMP: A Zero-D Z-Pinch Implosion Code | | | | | |
| 12 PERSONAL AUTHOR(S) Giuliani, J.L., Jr. and Rogerson, J. | | | | | |
| 13a TYPE OF REPORT Interim | | 13b TIME COVERED FROM _____ TO _____ | | 14. DATE OF REPORT (Year, Month, Day) 1989 April 25 | 15 PAGE COUNT 55 |
| 16 SUPPLEMENTARY NOTATION (See page 11) | | | | | |
| 17 COSATI CODES | | | 18 SUBJECT TERMS (Continue on reverse if necessary and identify by block number) | | |
| FIELD | GROUP | SUB-GROUP | Z-Pinch | | |
| | | | Computational physics | | |
| | | | Plasma radiation sources | | |
| 19 ABSTRACT (Continue on reverse if necessary and identify by block number) A new single zone, radiation-hydrodynamics code (ZPIMP) for modeling current driven gas puff implosions is developed. The hydrodynamics is based upon the finite difference equations for a standard multi-zone simulation. An analytic solution for the diffusion of the magnetic field in a moving medium is used to calculate the resistive heating and Maxwell stresses. A non-LTE ionization dynamics is self-consistently coupled to radiation transport for the single plasma zone. A circuit equation is solved for the input current to the plasma load. The problem of complete energy conservation in a numerical finite difference code is addressed in detail. The ZPIMP code is applied to the implosion of an aluminum vapor on GAMBLE II. A brief comparison of the results for annular shells and filled cylinders is presented. (JD) | | | | | |
| 20 DISTRIBUTION/AVAILABILITY OF ABSTRACT <input checked="" type="checkbox"/> UNCLASSIFIED/UNLIMITED <input type="checkbox"/> SAME AS RPT <input type="checkbox"/> DTIC USERS | | | 21 ABSTRACT SECURITY CLASSIFICATION UNCLASSIFIED | | |
| 22a NAME OF RESPONSIBLE INDIVIDUAL Dr. Jack Davis | | | 22b TELEPHONE (Include Area Code) (202) 767-3278 | 22c OFFICE SYMBOL Code 4720 | |

SECURITY CLASSIFICATION OF THIS PAGE

16. SUPPLEMENTARY NOTATION:

This research was sponsored by the Defense Nuclear Agency under Subtask Code and Title: RL RA/Advanced Simulation Concepts, Work Unit Code and Title, 00050, X-Ray Source Development Theory.

DD Form 1473, JUN 86 (Reverse)

SECURITY CLASSIFICATION OF THIS PAGE

CONTENTS

| | | |
|------|--|----|
| I. | INTRODUCTION | 1 |
| II. | DYNAMICS | 3 |
| | A. Magnetohydrodynamic Equations in Cylindrical Symmetry | 3 |
| | B. Integral Form of the Equations | 7 |
| | C. Finite Difference Form of the Equations | 10 |
| | D. Hydrodynamics for the Zero-D Model | 15 |
| | E. Magnetic Induction Equation | 17 |
| | F. Circuit Model | 21 |
| | G. Total Energy Conservation | 23 |
| III. | ATOMIC MODEL AND RADIATION TRANSPORT | 27 |
| IV. | AVERAGE-ATOM MODEL | 28 |
| V. | APPLICATION TO ALUMINUM VAPORS | 29 |
| | A. Plasma Shells of Varying Thickness | 29 |
| | B. Filled Cylinder Plasmas | 30 |
| VI. | SUMMARY | 31 |
| | ACKNOWLEDGEMENTS | 32 |
| | REFERENCES | 33 |
| | DISTRIBUTION LIST | 45 |



| | |
|------------------------|-------------------------------------|
| Accession No. | |
| FD-302 (Rev. 11-27-60) | <input checked="" type="checkbox"/> |
| DTIC Code | <input type="checkbox"/> |
| Unclassified | <input type="checkbox"/> |
| Justification | |
| By _____ | |
| Distribution/ | |
| Availability Codes | |
| Distribution/ | |
| Dist | Special |
| A-1 | |

ZPIMP: A ZERO-D Z-PINCH IMPLOSION CODE

I. INTRODUCTION

The discharge of electrical energy through a cylindrical gas puff is a well tested means of creating an intense burst of high energy radiation. Typical output from an imploding neon Z-pinch is a few kJ of x-rays when the peak current is about 1 MA on the GAMBLE II pulsed-power device at the Naval Research Laboratory. The experimental program to produce a bright and consistent Plasma Radiation Source (PRS) on GAMBLE II and on other facilities has evolved over the past several years. This program rapidly changes as new concepts in plasma load design are continually proposed. To predict the utility of, analyze, and revise such new ideas inexpensively, it is useful to model the proposed implosion in a simulation. A zero-dimensional radiation-hydrodynamics code provides both a succinct and rapid resource to address the above issues.

In a zero-D model of an axisymmetric implosion, the entire plasma is pictured to implode as a unit, either in an annular shell or a filled cylinder. The velocity of the imploding shell or cylinder is determined by the volume integral of the momentum or kinetic energy equation; the internal energy by the volume integral of the plasma energy equation. Several zero-D codes have been used in the past to predict and study Z-pinch dynamics. The code SIMPLODE was used to study neon^{2,3} and sodium⁴ implosions, while a similar code was employed by McDonald and Ottinger⁵ to also study a neon PRS. In the SIMPLODE code³ the mass density, velocity, and current density are taken as uniform across the annular shell. The waveform of the driving current waveform is a prescribed function of time, not determined from a circuit equation. The radiative cooling is based on a detailed non-LTE collisional-radiative equilibrium (CRE) model for the ionization dynamics. The escape probability approximation is used for the radiative transfer of the lines. The momentum equation determines the velocity of the imploding shell. Recent investigations with the SIMPLODE code indicate a serious

drawback, however: total energy is not always conserved. In the McDonald and Ottinger code⁵ the mass density in the plasma shell is uniform, while the velocity profile is determined from the continuity equation. The velocities of the inner and outer shell radii are equal. To maintain total energy conservation, the outer shell velocity is determined by the kinetic energy equation rather than the momentum equation. The current density is uniform but limited to a small skin region in the outer part of the plasma shell. Although the extent of this region of resistive heating evolves in time, it does so according to the local plasma velocity. Hence the same mass element is always carrying the current and no diffusion of the magnetic field is possible. The temperature of the skin is allowed to be different from that of the core region. The ionization state and radiative emissivity are determined from fits to a sample CRE calculation. Opacity effects on the radiative output were scaled with the load mass to match experimental data.

The present ZPIMP code is a new zero-D model which adopts the best aspects of the previous codes, namely the circuit equation and CRE ionization, while improving on the dynamics. For the hydrodynamic equations, this code is structured much like a typical multi-zone 1-D simulation code. In §II.A to §II.C the spatial and temporal finite difference forms of the hydrodynamic equations are derived in detail. These results are reduced to three zones in §II.D, with most of the mass contained in the central zone. This zone is characterized by an averaged density, ion temperature, and electron temperature. The finite difference approach to the hydrodynamics allows one to calculate separate velocities for the inner and outer radii of the shell. The steps in §II.D also point out the limitations of a zero-D code, particularly at the bounce time. For the evolution of the magnetic field, the induction equation is analytically solved (§II.E) for the magnetic flux in a moving medium. The solution assumes a small gradient length scale for the field and uses a planar geometry for the region of magnetic diffusion. As the plasma heats up and the resistivity decreases, the form of the solution displays the onset of flux freezing. A simple circuit model is employed in §II.F to self consistently determine the driving current from a supplied open circuit voltage. Section II.G addresses the problem of total plasma plus field energy conservation. The ionization dynamics is handled by a non-LTE CRE model (§III), and the probability-of-escape method for radiative transfer is used to handle opacity and trapping effects in the lines. At the start-up

of the simulation, where the temperatures are below 20 eV, the CRE model is replaced by an average-atom model as described in §IV. These last two sections are brief since the essential features have been described in previous papers.

As stated in the opening paragraph, the primary motivation for a zero-D simulation code is the rapid investigation of new concepts. For instance, recent interest has turned to imploding aluminum vapor puffs on the GAMBLE II device. In §V we apply the ZPIMP code to model such implosions. The implosion radius, maximum electron temperature, maximum charge state, and maximum continuum and line radiation is investigated. The initial geometry of the vapor is varied from annular puffs to filled cylinders. Detailed studies of various mass loadings and geometric configurations to determine the optimum radiative yields, emitted spectra from the L- and K-shells, and pulse durations will be presented in a following report.

A summary of the essential points of the report is contained in §VI.

II. DYNAMICS

A. Magnetohydrodynamic Equations in Cylindrical Symmetry.

The structure of the simulation code ZPIMP is modelled after the standard form of large scale radiation-hydrodynamic codes. The ionization dynamics and radiation transport is time split from the magneto-hydrodynamics, and communication between these two physical aspects is handled through a local radiative heating or cooling term. The ionization and radiation aspect will be discussed in §§ III and IV. In the present section we consider the magnetohydrodynamics of the Z-pinch and derive the appropriate equations for numerical simulations by starting from the general plasma-fluid equations. Let $\rho_i = m_i n_i$ ($\rho_e = m_e n_e$) be the ion (free electron) mass density; eZ_i the mean charge state of the ions; p_i (p_e) the ion (electron) pressure; and ϵ_i (ϵ_e) the ion (electron) internal energy. We will assume cylindrical symmetry (no ϕ -dependence) and axial invariance (no Z-dependence) so that all plasma and field variables depend only on the time t and the radial coordinate r . Furthermore, we assume for the mass weighted velocity $\mathbf{v} = v_R \mathbf{e}_R$, and for the magnetic field $\mathbf{B} = B_\phi \mathbf{e}_\phi$. The last assumption together with Ampere's law

implies $\mathbf{J} = J_Z \mathbf{e}_Z$ for the current density in the absence of displacement currents. Thus the electrons have the same velocity as the ions in the radial direction, vis. v_R , but unlike the ions, there must be a non-zero electron velocity in the axial direction.

We now write down the plasma and field equations subject to the above geometry. The mass continuity equation is

$$\frac{\partial \rho_i}{\partial t} + \frac{1}{r} \frac{\partial}{\partial r}(r \rho_i v_R) = 0. \quad (1)$$

The electron continuity equation is replaced by the requirement of charge neutrality, $n_e = n_i Z_i$.

The total momentum equation is found by adding the electron and ion momentum equations and neglecting the electron inertial terms:

$$\frac{\partial}{\partial t}(\rho_i v_R) + \frac{1}{r} \frac{\partial}{\partial r}(\rho_i v_R^2) + \frac{\partial}{\partial r}(p_i + p_e + Q_{vis}) = -\frac{1}{c} J_Z B_\phi. \quad (2)$$

In this equation Q_{vis} is an artificial viscosity term used to numerically smooth the conversion of kinetic energy to thermal energy at the bounce. Section II.C on finite differencing discusses the appropriate form for Q_{vis} .

The equation for the ion internal energy ϵ_i is

$$\frac{\partial}{\partial t}(\rho_i \epsilon_i) + \frac{1}{r} \frac{\partial}{\partial r}(r \rho_i \epsilon_i v_R) + (p_i + Q_{vis}) \frac{1}{r} \frac{\partial}{\partial r}(r v_R) + \frac{1}{r} \frac{\partial}{\partial r}(r q_{i,R}) = Q_{ie}. \quad (3)$$

In the present application we will be considering gaseous vapors so that the strong coupling effects of high density plasmas can be ignored. For an ideal perfect ion gas $\epsilon_i = (3/2)k_B T_i / m_i$. The thermal heat flux is

$$q_{i,R} = -\kappa_1^{(i)} \frac{\partial}{\partial r}(k_B T_i), \quad (4)$$

where $\kappa_1^{(i)}$ is the thermal conductivity given by Braginskii⁶ or Epperlein and Haines⁷. Since we are carrying separate ion and electron temperatures the energy transfer from the electrons to the ions is

$$Q_{ie} = 3 \frac{m_e}{m_i} \frac{n_e}{\tau_{ie}} k_B (T_i - T_e), \quad (5)$$

where τ_{ie} is the ion-electron collision time.

The equation for the electron internal energy ϵ_e is

$$\begin{aligned} \frac{\partial}{\partial t}(\rho_e \epsilon_e) + \frac{1}{r} \frac{\partial}{\partial r}(r \rho_e \epsilon_e v_R) + p_e \frac{1}{r} \frac{\partial}{\partial r}(r v_R) + \frac{1}{r} \frac{\partial}{\partial r}(r q_{e,R}) \\ = \Lambda - Q_{ie} + \eta_1 J_Z^2 + \frac{\beta_\Lambda}{en_e} J_Z \frac{\partial}{\partial r}(k_B T_e) . \end{aligned} \quad (6)$$

The specific electron internal energy is composed of two parts, the first component is due to the free electrons and the second is the electronic energy of excitation and ionization: $\epsilon_e = (3/2)k_B T_e/m_e + (\rho_i/\rho_e)\epsilon_{ex}$. The radiative heating rate, or cooling rate if negative, is contained in Λ . The quantities ϵ_{ex} and Λ are calculated prior to each hydrodynamic step and kept constant during that step. The electron heat flux is

$$q_{e,R} = -\kappa_1^{(e)} \frac{\partial}{\partial r}(k_B T_e) + k_B T_e \beta_\Lambda \text{sign}(B_\phi) \frac{J_Z}{en_e} . \quad (7)$$

The thermal transport coefficients $\kappa_1^{(e)}$, β_Λ , and α_1 are again given by Braginskii⁶, and we have expressed the resistivity as $\eta_1 = \alpha_1/e^2 n_e^2$. Also, $\text{sign}(B_\phi) = B_\phi/|B_\phi|$.

In place of the electron momentum equation a generalized Ohm's law for the plasma is derived by dropping the electron inertial terms and solving for the electric field. The Z-component is given by

$$E_Z = -\frac{1}{c} v_R B_\phi + \eta_1 J_Z + \frac{\beta_\Lambda}{en_e} \text{sign}(B_\phi) \frac{\partial}{\partial r}(k_B T_e) . \quad (8)$$

To complete the set of equations we have Faraday's law for the evolution of the magnetic field,

$$\frac{\partial B_\phi}{\partial t} = c \frac{\partial E_Z}{\partial r} , \quad (9)$$

and Ampere's law without the displacement current for the current density,

$$J_Z = \frac{c}{4\pi} \frac{1}{r} \frac{\partial}{\partial r}(r B_\phi) . \quad (10)$$

For later reference we present the equations for the plasma kinetic energy, plasma total energy, and field energy. Multiplying the total momentum equation by v_R and using the mass continuity equation leads to the plasma kinetic energy equation:

$$\frac{\partial}{\partial t} \left(\frac{1}{2} \rho_i v_R^2 \right) + \frac{1}{r} \frac{\partial}{\partial r} \left[r v_R \left(\frac{1}{2} \rho_i v_R^2 + p_i + p_e + Q_{\text{vis}} \right) \right] - (p_i + p_e + Q_{\text{vis}}) \frac{1}{r} \frac{\partial}{\partial r} (r v_R) = - \frac{v_R}{c} J_Z B_\phi. \quad (11)$$

Adding to this result both internal energy equations gives the total plasma energy equation:

$$\frac{\partial}{\partial t} \left(\rho_i \varepsilon_i + \rho_e \varepsilon_e + \frac{1}{2} \rho_i v_R^2 \right) + \frac{1}{r} \frac{\partial}{\partial r} \left[r v_R \left(\rho_i \varepsilon_i + \rho_e \varepsilon_e + \frac{1}{2} \rho_i v_R^2 + p_i + p_e + Q_{\text{vis}} \right) \right] + \frac{1}{r} \frac{\partial}{\partial r} (r q_i + r q_e) = \lambda + J_Z \left(- \frac{1}{c} v_R B_\phi + \eta_{\perp} J_Z + \frac{\beta_\lambda}{e n_e} \text{sign}(B_\phi) \frac{\partial}{\partial r} (k_B T_e) \right). \quad (12)$$

Poynting's theorem for the total magnetic field energy is readily derived from Faraday's law by multiplying by $B_\phi/4\pi$:

$$\frac{\partial}{\partial t} \left(\frac{B_\phi^2}{8\pi} \right) - \frac{c}{4\pi} \frac{1}{r} \frac{\partial}{\partial r} (r E_Z B_\phi) = - J_Z E_Z. \quad (13)$$

The above equations contain all the transport terms as given by Braginskii subject to the conditions of cylindrical symmetry and translational invariance along the axial direction. Following previous studies we will henceforth drop the thermal frictional component of the electric field (the term in β_λ) in comparison with the resistive component (the term in η_{\perp}) in eqns (6), (8), and (12). For $J_Z \sim I/2\pi R\delta$, where I is the current, R is the plasma radius and δ is an effective skin depth, the neglect of the frictional component is valid as long as

$$I \gg \frac{620}{Z_i \ln(\lambda)} \left(\frac{\alpha_1}{\beta_\lambda^0} \right) T_e^{3/2} \left| \frac{\partial T_e}{\partial r} \right| R \delta \text{ amps.}$$

In this condition temperatures are in eV, distances in cm, and $\alpha_{\perp}^{\circ}/\beta_{\Lambda}^{\circ}$ is a factor of order unity depending on $(eB_{\phi}/m_e c)\tau_{ie}$ and Z_i .

B. Integral Form of the Equations.

In a zero-D, cylindrically symmetric, radiation-hydrodynamic simulation code the basic assumption is that most or all of the plasma is confined to an annulus or filled cylinder. The equations derived above are then applied to this plasma region as a whole with the radial dependence of the plasma variables either assumed a priori or integrated out. For instance, one could begin by specifying a density and velocity profile consistent with the mass continuity equation. These profiles would depend on a Lagrangian coordinate spanning the plasma shell, the inner (R_{in}) and outer (R_{out}) shell radii, and the inner (V_{in}) and outer (V_{out}) shell velocities. The momentum equation is next integrated over the shell volume to obtain an equation for V_{out} . Likewise, the internal energy equation is integrated over the shell volume to obtain an expression for the average internal energy. This approach was employed by Guillory and Terry². McDonald and Ottinger⁵, however, found that the total plasma plus field energy was not conserved in the Guillory and Terry model. Instead, McDonald and Ottinger employed the kinetic energy equation to determine V_{out} , with the assumption $V_{in} = V_{out}$. Further, within the plasma shell they considered two subzones which differed in temperature but not density: an outer zone from $R_{out} - \delta$ to R_{out} of fixed mass which contained a uniform current density, and an inner zone from R_{in} to $(R_{out} - \delta)$ which was current free.

An alternative approach is to view a zero-D model as a special case of a typical full 1-D code with many zones. In this approach no plasma profiles are assumed a priori, instead (i) the fluid is divided into a number of zones such that each zone boundary moves with the fluid velocity at that interface, and (ii) spatially averaged values for the plasma variables are used in each zone. The definition of the averaged quantities are determined by approximations to the volume integrals of the fluid equations. Since the integration is over a moving zone it is appropriate to adopt a Lagrangian

framework for the fluid equations. This requires the transformation of the independent variable from the spatial coordinate r to an indexing coordinate j , wherein each fluid element moves about between fixed values of j . The spatial position of a fluid interface with index j is $R(j)=R_j$, and its velocity is $DR_j/Dt = V_j$. The Z-axis is at $j=0$ and the outermost interface is at $j=NJ$. The Jacobian for the transformation between the two coordinate is $\theta = \partial R/\partial j$, giving for the volume element about j , $2\pi\Delta Z R dR = 2\pi\Delta Z R(j)\theta(j) dj$. To integrate the dynamic equations we regularly employ the theorem,

$$\int_{R(j)}^{R(j+1)} \frac{\partial f}{\partial t} 2\pi R \theta dj = \frac{D}{Dt} \int_{R(j)}^{R(j+1)} f 2\pi r dr = \left[2\pi R \frac{DR}{Dt} f \right]_{R(j)}^{R(j+1)}, \quad (14)$$

where f is an arbitrary quantity. We note that the meaning of Df/Dt is that the function f is first to be written as a function of the Lagrangian coordinate j and the time t before differentiating. The relation above is then readily proven by transforming the integral on the right to a function of j ($2\pi r dr \rightarrow 2\pi R \theta dj$), bringing in the time derivative and finally using the standard relation between the Lagrangian and Eulerian time derivative:

$$\frac{Df}{Dt} = \frac{\partial f}{\partial t} + \frac{V_R}{\theta} \frac{\partial f}{\partial j}.$$

We now integrate the continuity, momentum, and energy equations over a volume element $2\pi R \theta dj$ and apply eqn.(14). For the continuity equation (1) one finds

$$\frac{D}{Dt} \int_{R(j)}^{R(j+1)} \rho_i 2\pi r dr + \left[2\pi R \rho_i \left(V_R - \frac{DR}{Dt} \right) \right]_{R(j)}^{R(j+1)} = 0, \quad (15)$$

which is the simple fact that the total mass between Lagrangian coordinates j and $j+1$ is constant since the grid velocity, DR/Dt , equals the mass velocity, V_R . In the volume integral of the total momentum equation (2) we use different upper and lower bounds:

$$\frac{D}{Dt} \int_{R(j-1/2)}^{R(j+1/2)} \rho_i v_R^2 2\pi r dr + \int_{j-1/2}^{j+1/2} \frac{\partial}{\partial j} (\rho_i + \rho_e + Q_{vis}) 2\pi R dj = - \int_{R(j-1/2)}^{R(j+1/2)} \frac{1}{c} J_Z B_\phi 2\pi r dr. \quad (16)$$

For the ion internal energy equation (3) we use the same limits as in the continuity equation:

$$\frac{D}{Dt} \int_{R(j)}^{R(j+1)} \rho_i \epsilon_i 2\pi r dr + \int_j^{j+1} (\rho_i + Q_{vis}) \frac{\partial}{\partial j} (RV_R) 2\pi dj + \left[2\pi R q_{i,R} \right]_{R(j)}^{R(j+1)} = \int_{R(j)}^{R(j+1)} Q_{ie} 2\pi r dr. \quad (17)$$

Likewise, the volume integral of the electron internal energy (6) is

$$\begin{aligned} \frac{D}{Dt} \int_{R(j)}^{R(j+1)} \rho_e \epsilon_e 2\pi r dr + \int_j^{j+1} \rho_e \frac{\partial}{\partial j} (RV_R) 2\pi dj + \left[2\pi R q_{e,R} \right]_{R(j)}^{R(j+1)} \\ = \int_{R(j)}^{R(j+1)} \left[\lambda - Q_{ie} + \eta_\perp J_Z^2 \right] 2\pi r dr. \quad (18) \end{aligned}$$

Again for later reference we list the volume integral of the kinetic energy equation (11),

$$\begin{aligned} \frac{D}{Dt} \int_{R(j-1/2)}^{R(j+1/2)} \frac{1}{2} \rho_i v_R^2 2\pi r dr + \left[(\rho_i + \rho_e + Q_{vis}) 2\pi R V_R \right]_{R(j-1/2)}^{R(j+1/2)} \\ - \int_{R(j-1/2)}^{R(j+1/2)} (\rho_i + \rho_e + Q_{vis}) \frac{1}{r} \frac{\partial r V_R}{\partial r} 2\pi r dr = - \int_{R(j-1/2)}^{R(j+1/2)} \frac{1}{c} v_R J_Z B_\phi 2\pi r dr; \quad (19) \end{aligned}$$

the integral of the plasma energy equation (12) between arbitrary boundaries $R(j=a)$ and $R(j=b)$,

$$\frac{D}{Dt} \int_{R(j=a)}^{R(j=b)} \left(\rho_i \epsilon_i + \rho_e \epsilon_e + \frac{1}{2} \rho_i v_R^2 \right) 2\pi r dr + \left[(\rho_i + \rho_e + Q_{vis}) 2\pi R V_R \right]_{R(j=a)}^{R(j=b)}$$

$$+ \left[2\pi R q_{i,R} + 2\pi R q_{e,R} \right]_{R(j=a)}^{R(j=b)} = \int_{R(j=a)}^{R(j=b)} \left(\Lambda - \frac{v_R}{c} J_Z B_\phi + \eta_\perp J_Z^2 \right) 2\pi r dr; \quad (20)$$

and the integral of the field energy equation (13) with the same boundaries,

$$\frac{D}{Dt} \int_{R(j=a)}^{R(j=b)} \left(\frac{B_\phi^2}{8\pi} \right) 2\pi r dr - \left[\left(\frac{B_\phi^2}{8\pi} \right) 2\pi R v_R + \frac{c}{4\pi} E_Z B_\phi \right]_{R(j=a)}^{R(j=b)} = - \int_{R(j=a)}^{R(j=b)} J_Z E_Z 2\pi r dr. \quad (21)$$

C. Finite Difference Form of the Equations.

The basic set of equations which are used to advance the density, velocity, and internal energies are eqns.(15)-(18). We next convert this set from time differential and spatially integrated forms to true finite difference forms. The mass continuity equation (15) determines the advanced average density of each zone:

$$\rho_{i,j+1/2}^{(n+1)} = \frac{M_{j+1/2}(t=t^{n+1})}{Vol_{j+1/2}^{(n+1)}} = \frac{M_{j+1/2}(t=0)}{\Delta Z \pi \left[(R_{j+1}^{(n+1)})^2 - (R_j^{(n+1)})^2 \right]}, \quad (22)$$

where $M_{j+1/2}$ is the total mass initially between R_j and R_{j+1} , and t^n is the time at step n .

For the total momentum equation we take V_j to be the mass weighted velocity at interface R_j between $R_{j+1/2}$ and $R_{j-1/2}$ and approximate eqn. (16) as

$$\left(\frac{M_{j+1/2} + M_{j-1/2}}{2\Delta Z} \right) \frac{v_j^{(n+1)} - v_j^{(n)}}{\Delta t} + \left[(P_{j+1/2} - P_{j-1/2}) 2\pi R_j \right]^{(n+1/2)} = - \left[\int_{R(j-1/2)}^{R(j+1/2)} \frac{1}{c} J_Z B_\phi 2\pi r dr \right]^{(n+1/2)}, \quad (23)$$

where

$$P = p_i + p_e + Q_{vis}$$

In this approximation we have associated half of the total mass in each of the adjacent zones with the velocity at the interface j . The integral over the pressure force is evaluated for a step function approximation to the pressure profile across the interface. The temporal finite differencing is indicated by the superscripts $(n+1)$ and (n) . The superscript $(n+1/2)$ does not denote the time average of a quantity, but rather a value determined from a half-step predictor.

The form of the artificial viscosity is

$$Q_{vis,j+1/2} = b_{vis} \rho_{i,j+1/2} C_{s,j+1/2} \min\{0, V_j - V_{j+1}\}$$

where b_{vis} is a constant parameter chosen to match the results from a standard multi-zone hydrodynamic code. C_s is the isothermal sound speed of the ions. Note that the artificial viscous pressure only contributes if the zone is undergoing compression.

For eqns.(17) and (18) we take the ion and electron internal energies as uniform between R_j and R_{j+1} . Equation (17) is approximated as

$$\begin{aligned} \frac{M_{j+1/2}}{\Delta Z} \frac{\epsilon_{i,j+1/2}^{(n+1)} - \epsilon_{i,j+1/2}^{(n)}}{\Delta t} + (p_i + Q_{vis})_{j+1/2}^{(n+1/2)} \left(2\pi R_{j+1}^{(n+1/2)} V'_{j+1} - 2\pi R_j^{(n+1/2)} V'_j \right) \\ + \left[2\pi R_{j+1} q_{i,j+1} - 2\pi R_j q_{i,j} \right]^{(n+1)} = \left[\bar{Q}_{ie} \frac{Vol}{\Delta Z} \right]_{j+1/2}^{(n+1/2)}, \quad (24) \end{aligned}$$

where \bar{Q}_{ie} is to be evaluated using the spatially averaged temperature and density according to eqn.(5). The pressure integral of eqn.(17) has obviously been approximated by extracting the averaged pressure of zone $j+1/2$ and then carrying out the integral. The temporal location of the heat flux is at the advanced time, for in practice one time splits off this term and calculates its effect implicitly after advancing the energy equation to t^{n+1} . We have also not yet specified the time location of V'_j and V'_{j+1} in the second term of this equation, but will do so shortly by an energy conservation relation. The corresponding result for the electron internal energy equation (18) is

$$\begin{aligned}
& \frac{M_{e,j+1/2}}{\Delta Z} \frac{\epsilon_{e,j+1/2}^{(n+1)} - \epsilon_{e,j+1/2}^{(n)}}{\Delta t} + p_{e,j+1/2}^{(n+1/2)} \left(2\pi R_{j+1}^{(n+1/2)} v'_{j+1} - 2\pi R_j^{(n+1/2)} v'_j \right) \\
& + \left[2\pi R_{j+1} q_{e,j+1} - 2\pi R_j q_{e,j} \right]^{(n+1)} \\
& = \left[(\bar{\lambda} - \bar{Q}_{ie}) \frac{Vol}{\Delta Z} \right]_{j+1/2}^{(n+1/2)} + \left[\int_{R(j)}^{R(j+1)} \eta_{\perp} J_Z^2 2\pi r dr \right]^{(n+1/2)}, \quad (25)
\end{aligned}$$

where $A^{(n+1/2)}$ is the average heating (cooling if negative) rate over the timestep. The same statements concerning the time location of v'_j , v'_{j+1} , and the heat flux terms made for the ion internal energy equation apply to this equation. Note that the total number of electrons in zone $j+1/2$ has been assumed to be a constant in this approximation. This reflects the time splitting between ionization and hydrodynamics wherein the number of free electrons is unchanged during a hydro-step. This approach requires that the total electron internal energy, $(3/2)M_e k_B T_e / m_e + M \epsilon_{ex}$, remain unchanged during an ionization step.

The approximation to the integrals made in the above equations are not arbitrary, but are determined by plasma energy conservation over the entire system within the finite difference scheme. We now derive through algebraic manipulations a plasma energy conservation relation starting from the finite difference forms used to advance the velocity [eqn.(23)] and the internal energies [eqns.(24) and (25)]. The result will then be compared with the exact conservation equation (20) as a check on the finite difference forms (23)-(25). Define

$$\langle v_j \rangle \equiv \frac{1}{2} \left(v_j^{(n+1)} + v_j^{(n)} \right), \quad (26)$$

and likewise for $\langle v_{j+1/2} \rangle$. This time averaged velocity at R_j is not necessarily the same as $v_j^{(n+1/2)}$, which is the result of a half-step predictor. Next multiply the finite difference form of the total momentum equation (23) by $\langle v_j \rangle$ to obtain

$$\frac{1}{2} \left(\frac{M_{j+1/2} + M_{j-1/2}}{2\Delta Z} \right) \frac{1}{\Delta t} \left[(v_j^{(n+1)})^2 - (v_j^{(n)})^2 \right] + \left(P_{j+1/2}^{(n+1/2)} - P_{j-1/2}^{(n+1/2)} \right) 2\pi R_j^{(n+1/2)} \langle v_j \rangle = - \langle v_j \rangle \left[\int_{R(j-1/2)}^{R(j+1/2)} \frac{1}{c} J_z B_\phi 2\pi r dr \right]^{(n+1/2)}. \quad (28)$$

This relation is the derived finite difference form of the kinetic energy equation. If we note that

$$\begin{aligned} \left(P_{j+1/2}^{(n+1/2)} - P_{j-1/2}^{(n+1/2)} \right) 2\pi R_j^{(n+1/2)} \langle v_j \rangle &= \left[P_{j+1/2}^{(n+1/2)} 2\pi R_{j+1/2}^{(n+1/2)} \langle v_{j+1/2} \rangle - P_{j-1/2}^{(n+1/2)} 2\pi R_{j-1/2}^{(n+1/2)} \langle v_{j-1/2} \rangle \right] \\ &- P_{j+1/2}^{(n+1/2)} \left(2\pi R_{j+1/2}^{(n+1/2)} \langle v_{j+1/2} \rangle - 2\pi R_j^{(n+1/2)} \langle v_j \rangle \right) \\ &- P_{j-1/2}^{(n+1/2)} \left(2\pi R_j^{(n+1/2)} \langle v_j \rangle - 2\pi R_{j-1/2}^{(n+1/2)} \langle v_{j-1/2} \rangle \right), \end{aligned}$$

then the form of the terms on the left hand side of equation (28) is consistent with those same terms in equation (19). Equation (28) thus expresses the local conservation of kinetic energy over the domain $R_{j-1/2}$ to $R_{j+1/2}$. On the other hand, the sum of eqns. (24) and (25) expresses the local conservation of total internal energy over the domain R_j to R_{j+1} . Since the two domains are different we cannot derive a finite difference form for local conservation of total plasma energy (eqn. 20) starting from the finite differenced momentum and internal energy equations. However, total plasma energy can be shown to be globally conserved. To see this sum equation (28) over the interfaces between the axis and the outer boundary ($0 < j < NJ$) and rearrange the result to read

$$\begin{aligned} \frac{1}{\Delta t} \sum_{j=0}^{NJ-1} \frac{1}{2} \frac{M_{j+1/2}}{\Delta Z} \frac{1}{2} \left[(v_{j+1}^{(n+1)})^2 + (v_j^{(n+1)})^2 - (v_{j+1}^{(n)})^2 - (v_j^{(n)})^2 \right] \\ - \sum_{j=0}^{NJ-1} P_{j+1/2}^{(n+1/2)} \left(2\pi R_{j+1}^{(n+1/2)} \langle v_{j+1} \rangle - 2\pi R_j^{(n+1/2)} \langle v_j \rangle \right) \end{aligned}$$

$$= \sum_{j=0}^{NJ-1} \langle v_j \rangle \left[\int_{R(j-1/2)}^{R(j+1/2)} \frac{1}{c} J_Z B_\phi 2\pi r dr \right]^{(n+1/2)}, \quad (29)$$

as long as $V(j=0) = V(j=NJ) = 0$. Next sum the internal energy equations (24) and (25) from $j=0$ to $j=NJ-1$ and add to equation (29). We now identify V'_j in eqns.(24) and (25) with $\langle v_j \rangle$. At the axis one must have $q_{i,R} = q_{e,R} = 0$, and we will assume that there is no energy loss due to conduction through the outer wall at $j = NJ$. Then the result is

$$\begin{aligned} & \frac{1}{\Delta t} \sum_{j=0}^{NJ-1} \frac{1}{2} \frac{M_{j+1/2}}{\Delta Z} \frac{1}{2} \left[\left(v_{j+1}^{(n+1)} \right)^2 + \left(v_j^{(n+1)} \right)^2 - \left(v_{j+1}^{(n)} \right)^2 - \left(v_j^{(n)} \right)^2 \right] \\ & + \frac{1}{\Delta t} \sum_{j=0}^{NJ-1} \frac{M_{j+1/2}}{\Delta Z} \left(\epsilon_{i,j+1/2}^{(n+1)} - \epsilon_{i,j+1/2}^{(n)} + \epsilon_{e,j+1/2}^{(n+1)} - \epsilon_{e,j+1/2}^{(n)} \right) \\ = & \sum_{j=0}^{NJ-1} \left[\left(\bar{\lambda} \frac{Vol}{\Delta Z} \right)_{j+1/2} + \int_{R(j)}^{R(j+1)} \eta_{\perp} J_Z^2 2\pi r dr - \langle v_j \rangle \int_{R(j-1/2)}^{R(j+1/2)} \frac{1}{c} J_Z B_\phi 2\pi r dr \right]^{(n+1/2)}. \quad (30) \end{aligned}$$

This expression is the derived finite difference form of the total plasma energy equation for the entire domain. Note the similarity of this result with the sum over all the zones of the exact expression, eqn.(20).

Equation (30) is actually quite remarkable for the case of no magnetic fields. It states that one can transport internal energies in a Lagrangian code and yet maintain global conservation for the total energy (internal + kinetic). This result is not based upon an expansion for a small timestep, but rather arises from the finite difference forms (23)-(25) for the momentum and internal energy equations. The proper sequence of steps to achieve energy conservation in a hydrodynamic system is as follows;

- (s-i) Using the values at $t^{(n)}$ do a half-step predictor to find ρ_i , V , ϵ_i , ϵ_e at $t^{n+1/2}$ for each j .
- (s-ii) From these quantities compute p_i , p_e , Q_{vis} , and R at $t^{n+1/2}$ at each j . (If there is a magnetic field, also compute the currents I and J_Z and the field B_ϕ at $t^{n+1/2}$ as discussed below.)
- (s-iii) Compute $V^{(n+1)}$ at each j from eqn.(23).

(s-iv) Form $\langle V_j \rangle$ from eqn.(26).

(s-v) Use these quantities in the energy eqns.(24) and (25) to find the final advanced quantities $\epsilon_i^{(n+1)}$ and $\epsilon_e^{(n+1)}$ at each j.

Unfortunately, with the addition of magnetic fields and an external circuit, conservation of the total plasma plus field energy is not as straight forward as it is for a hydrodynamic system. We have evaluated the $\mathbf{J} \times \mathbf{B}$ force term in eqn.(23) and the resistive heating term in eqn.(25) at $t^{n+1/2}$, but have yet to show consistency with the derived plasma plus field energy conservation. We will address this problem in §II.G.

D. Hydrodynamics for the Zero-D Model.

One of the objectives in deriving the above general equations is to explicitly demonstrate the underlying assumptions and limitations of a zero-D dynamic model. To reduce the above set of equations to two momentum and two internal energy equations, begin by considering three zones for the annular shell plasma. The inner zone extends from the axis at $j=0$ to $j=1$ (R_1), the central zone from $j=1$ (R_1) to $j=2$ (R_2), and the outer zone from $j=2$ (R_2) to $j=3$ (R_3). This last radius is that of a fixed cylindrical boundary termed the wall. The following assumptions are made;

(a-i) The total mass of the central zone ($j = 1+1/2$) dominates the mass of the inner and outer zones, $M_{1/2} \ll M_{3/2} \gg M_{5/2}$.

(a-ii) The temperatures of all three zones are nearly equal.

(a-iii) The ion and electron number densities of the central zone are always much larger than those of the inner and outer zones.

(a-iv) The outer zone is current free: $J_z = 0$ and $B_\phi = 2I/rc$ for $r > R_2$.

Since $Q_{vis} \propto \rho_i C_s \Delta V$, (a-ii) and (a-iii) also imply that the viscous pressure of the central zone likewise dominates. For an ideal gas law the same condition holds for the thermal pressures and the total internal energies (Me) of the central zone. Under these assumptions the momentum equations from eqn.(23) for V_1 and V_2 can be written as

$$\frac{M_{3/2}}{2\Delta Z} \frac{v_1^{(n+1)} - v_1^{(n)}}{\Delta t} + p_{3/2}^{(n+1/2)} 2\pi R_1^{(n+1/2)} = - \left[\int_{R(j=1/2)}^{R(j=3/2)} \frac{1}{c} J_z B_\phi 2\pi r dr \right]^{(n+1/2)}, \quad (31a)$$

and

$$\frac{M_{3/2}}{2\Delta Z} \frac{v_2^{(n+1)} - v_2^{(n)}}{\Delta t} - p_{3/2}^{(n+1/2)} 2\pi R_2^{(n+1/2)} = - \left[\int_{R(j=3/2)}^{R(j=2)} \frac{1}{c} J_z B_\phi 2\pi r dr \right]^{(n+1/2)}, \quad (31b)$$

The upper limit of this last integral stops at R_2 according to (a-iv). To eliminate the heat flux terms in the internal energy equations we separately sum eqns.(24) and (25) over all three zones. Assumptions (i) and (ii) allow us to write these sums as

$$\begin{aligned} \frac{M_{3/2}}{\Delta Z} \frac{\epsilon_{i,3/2}^{(n+1)} - \epsilon_{i,3/2}^{(n)}}{\Delta t} + (p_i + Q_{vis})_{3/2}^{(n+1/2)} \left(2\pi R_2^{(n+1/2)} \langle v_2 \rangle - 2\pi R_1^{(n+1/2)} \langle v_1 \rangle \right) \\ = \left[\bar{Q}_{ie} \frac{Vol}{\Delta Z} \right]_{j=3/2}^{(n+1/2)}, \quad (32a) \end{aligned}$$

and

$$\begin{aligned} \frac{M_{e,3/2}}{\Delta Z} \frac{\epsilon_{e,3/2}^{(n+1)} - \epsilon_{e,3/2}^{(n)}}{\Delta t} + p_{e,3/2}^{(n+1/2)} \left(2\pi R_2^{(n+1/2)} \langle v_2 \rangle - 2\pi R_1^{(n+1/2)} \langle v_1 \rangle \right) \\ = \left[(\bar{\lambda} - \bar{Q}_{ie}) \frac{Vol}{\Delta Z} \right]_{j=3/2}^{(n+1/2)} + \left[\int_{R=0}^{R(2)} \eta_\perp J_z^2 2\pi r dr \right]^{(n+1/2)}. \quad (32b) \end{aligned}$$

The radiative term λ only contributes from the central zone since it has the dominant number of radiators. The ion-electron energy exchange term only contributes from the central zone since $Q_{ie} \propto n_e^2$.

The assumption (a-ii) is reasonable as long as the heat transfer, particularly due to the ion heat flux, is large compared to the compressional heating: $3.9\tau_{ii} \Delta(k_B T_i / m_i) / \Delta r^2 \gg \Delta v / \Delta r$. However, assumptions (a-ii) and (a-iii) do break down when the plasma shell bounces off the axis. The pressure of the inner zone must then rise above that of the central zone as the

collapse is reversed. Further, if there is some anomalous resistivity in the outer low density zone, then assumption (a-iv) may also be violated.

Equations (22), and (31a)-(32b) are the reduced set of equations for advancing the hydrodynamic quantities of an imploding shell in our zero-D code. In the case of a filled plasma cylinder the interface at $j=1$ is identified with the Z-axis. The momentum equation (31a) for V_1 is no longer needed and the internal energy equations determine ϵ_i and ϵ_e in the region between the Z-axis and R_2 . The problem with assumptions (a-ii) and (a-iii) at the time of the bounce has essentially been integrated away.

E. Magnetic Induction Equation.

One of the most important dynamical effects in a Z-pinch is the amount of resistive heating inside the plasma during the run-in phase. This is a consequence of the diffusion of the magnetic field from the outer plasma boundary into the collapsing plasma shell. Rather than fix a skin depth or define a current density profile in the plasma shell, we will develop an approximate solution for the magnetic diffusion in the moving plasma. The induction equation describing the diffusion is found by substituting the expression for E_z from Ohm's law, eqn.(8), into Faraday's law, eqn.(9), and using the expression for J_z from eqn. (10):

$$\frac{\partial B_\phi}{\partial t} = - \frac{\partial}{\partial r}(v_R B_\phi) + \frac{\partial}{\partial r} \left[\frac{c^2 \eta_\perp}{4\pi} \left(\frac{B_\phi}{r} + \frac{\partial B_\phi}{\partial r} \right) \right], \quad (33)$$

where we have dropped the thermal friction term in β_Λ for the reason stated below eqn.(13). To solve eqn.(33) we make several additional assumptions to those listed in §II.D;

- (a-v) The current skin depth (δ) inside R_2 is sufficiently small that $B_\phi/r \ll \partial B_\phi/\partial r$.
- (a-vi) The resistivity is spatially uniform over the diffusing region, $\eta_\perp = \eta_\perp(t)$.

To convert this equation from an Eulerian framework to a Lagrangian one note that

$$\frac{\partial B_\phi}{\partial t} + \frac{\partial}{\partial r}(v_R B_\phi) = \frac{\partial B_\phi}{\partial t} + v_R \frac{\partial B_\phi}{\partial r} + \frac{B_\phi}{\theta} \frac{\partial v_R}{\partial j} = \frac{DB_\phi}{Dt} + \frac{B_\phi}{\theta} \frac{D\theta}{Dt} = \frac{1}{\theta} \frac{D\theta B_\phi}{Dt}$$

Finally, note the specific relation

$$R(j,t) = R_1(t) + (R_2(t) - R_1(t))j \Rightarrow \theta = \frac{\partial R}{\partial j} = R_2(t) - R_1(t) = \Delta R. \quad (34)$$

Equation (33) can now be written as

$$\frac{D\theta B_\phi}{Dt} = \frac{c^2 \eta_\perp}{4\pi\theta^2} \frac{\partial^2 \theta B_\phi}{\partial j^2}. \quad (35)$$

Note that if $\eta_\perp = 0$ for $t > t_1$, this equation states that the magnetic flux $\Delta Z \Delta R B_\phi$ remains fixed at its t_1 value even though ΔR may continue to change. Next transform to a new time variable:

$$\tau = \int_0^t \frac{c^2 \eta_\perp(t')}{4\pi\theta^2(t')} dt', \quad (36)$$

and thereby reduce eqn.(33) to a planar diffusion equation:

$$\frac{D(\theta B_\phi)}{D\tau} = + \frac{\partial^2 (\theta B_\phi)}{\partial j^2}. \quad (37)$$

The solution is subject to the initial and boundary conditions

$$\theta B_\phi = 0 \text{ at } \tau = 0 \quad \text{and} \quad \theta B_\phi = \theta(\tau) \frac{2I(\tau)}{R_2(\tau)c} \text{ at } j = 2 \text{ (} r=R_2 \text{)}, \quad (38)$$

The boundary condition at the outer plasma radius reflects the value of the magnetic field in the outer vacuum adjacent to the plasma due to the current I within the plasma. Equation (37) can be solved by the method of Laplace transforms. The result for the magnetic flux is

$$\Theta(\tau)B_{\phi}(j, \tau) = \frac{(2-j)}{2\sqrt{\pi}} \int_0^{\tau} \left(\Theta(\tau') \frac{2I(\tau')}{R_2(\tau')c} \right) \frac{e^{-(2-j)^2/4(\tau-\tau')}}{(\tau-\tau')^{3/2}} d\tau'. \quad (39)$$

For the following manipulations set

$$\Phi(\tau) \equiv \Theta(\tau) \frac{2I(\tau)}{R_2(\tau)c}. \quad (40)$$

In order to make the solution (39) tractable for numerical computation we will take Φ to be constant over each time interval (t^n, t^{n+1}) , and denote its value at $\tau^{n+1/2}$ by $\Phi_{n+1/2}$. Equation (39) can then be written as

$$\begin{aligned} \Theta(\tau)B_{\phi}(\tau) &= \frac{(2-j)}{2\sqrt{\pi}} \Phi_{N+1/2} \int_{\tau^N}^{\tau} \frac{e^{-(2-j)^2/4(\tau-\tau')}}{(\tau-\tau')^{3/2}} d\tau' \\ &+ \sum_{n=0}^{N-1} \frac{(2-j)}{2\sqrt{\pi}} \Phi_{n+1/2} \int_{\tau^n}^{\tau^{n+1}} \frac{e^{-(2-j)^2/4(\tau-\tau')}}{(\tau-\tau')^{3/2}} d\tau'. \end{aligned}$$

Next making the change of variables from τ' to $\psi = (2-j)/[2\sqrt{(\tau-\tau')}]$, the solution can be calculated at time $\tau^{N+1} > \tau > \tau^N$ from

$$\Theta(\tau)B_{\phi}(j, \tau) = \Phi_{N+1/2} \left[1 - \operatorname{erf} \left(\frac{2-j}{\alpha_N} \right) \right] + \sum_{n=0}^{N-1} \Phi_{n+1/2} \left[\operatorname{erf} \left(\frac{2-j}{\alpha_{n+1}} \right) - \operatorname{erf} \left(\frac{2-j}{\alpha_n} \right) \right], \quad (41)$$

where $\operatorname{erf}(x)$ is the error function and $\alpha_n \equiv 2\sqrt{(\tau-\tau^n)}$. Note that $\alpha_0 = 2\sqrt{\tau} > \alpha_1 > \dots > \alpha_N$.

One can interpret this last equation by noting that at the time step $\tau_{n+1/2}$, a component of the magnetic flux $\Phi_{n+1/2}$ enters the plasma and the diffusion length scale from that time on is $R_2\alpha_n$. Clearly at the outer radius where $j = 2$ the boundary condition eqn.(38) is satisfied, and at the initial instant when $\alpha_0 = 0$ there is no magnetic flux in the plasma.

For the current density $4\pi J_Z/c = B_{\phi}/R + (\partial B_{\phi}/\partial j)/\Theta$ one can calculate directly

$$J_Z = \frac{c}{4\pi} \frac{B_\phi}{R} + \frac{c}{2\pi^{3/2}\theta^2} \left[\sum_{n=1}^N (\phi_{n+1/2} - \phi_{n-1/2}) \frac{e^{-(2-j)^2/\alpha_n^2}}{\alpha_n} + \phi_{1/2} \frac{e^{-(2-j)^2/\alpha_0^2}}{\alpha_0} \right]. \quad (42)$$

A maximum for the skin depth δ of the current in the plasma shell at "time" τ can be determined by the penetration depth of the first component of the magnetic flux $\phi_{1/2}$ to enter the plasma at time $\tau=0$: $\delta \sim \alpha_0(R_2 - R_1)$. This value is clearly an overestimate of the skin depth since the magnetic flux components which enters the plasma shell at later times, $\phi_{n+1/2}$, are significantly larger and have a smaller penetration depth.

The total current within the radius R_2 at a time τ lying in the interval (τ^N, τ^{N+1}) is

$$I(\tau) = \int_1^2 J_Z(2-j, \tau) 2\pi [R_2(\tau) - (2-j)\theta(\tau)] \theta dj.$$

In the limit of a narrow skin depth one can neglect the second term in the square brackets in the integrand and the lower limit of the integral can be replaced by $-\infty$. One then finds by carrying out the integration the consistent result $I(\tau) = I_{N+1/2}$. Under the same estimates for computing the integral, the resistive heating at time $\tau^{n+1/2}$ in the electron internal energy equation (32b) is explicitly

$$\begin{aligned} \int_{-\infty}^2 \eta_1 J_Z^2 2\pi R \theta dj &= \eta_1 \frac{c^2 R_2}{4\pi^2 \theta^3} \left(\frac{\pi}{2}\right)^{1/2} \left[\left(\frac{\phi_{1/2}}{\alpha_0}\right)^2 + \sum_{n=1}^N (\phi_{n+1/2} - \phi_{n-1/2})^2 \frac{1}{\alpha_n} \right. \\ &+ \sum_{n=1}^N \sum_{\substack{m=1 \\ n \neq m}}^N (\phi_{n+1/2} - \phi_{n-1/2})(\phi_{m+1/2} - \phi_{m-1/2}) \frac{2\sqrt{2}}{(\alpha_n^2 + \alpha_m^2)^{1/2}} \\ &\left. + \sum_{n=1}^N \phi_{1/2} (\phi_{n+1/2} - \phi_{n-1/2}) \frac{2\sqrt{2}}{(\alpha_n^2 + \alpha_0^2)^{1/2}} \right]. \quad (43) \end{aligned}$$

Likewise the mean value for the magnetic field within R_0 is

$$\langle B_\phi \rangle = \frac{1}{R_2} \int_{-\infty}^2 B_\phi \Theta dj \approx \frac{1}{R_2 \sqrt{\pi}} \left[\phi_{N+1/2} \alpha_N + \sum_{n=0}^{N-1} \phi_{n+1/2} (\alpha_{n+1} - \alpha_n) \right]. \quad (44)$$

The Maxwell stresses of eqn. (31a) and (31b) can be readily evaluated in this limit:

$$\begin{aligned} \int_{3/2}^2 \left(-\frac{1}{c} J_z B_\phi \right) 2\pi R \Theta dj &= -\frac{1}{2} \int_{3/2}^2 \left(\frac{B_\phi}{R} + \frac{1}{\Theta} \frac{\partial B_\phi}{\partial j} \right) B_\phi (R_2 - (2-j)\Theta) \Theta dj \\ &= -\frac{1}{4} R_2 \left[B_\phi^2(j=2) - B_\phi^2(j=3/2) \right] = -\frac{I^2}{R_2^2 c} + \frac{1}{4} R_2 B_\phi^2(j=3/2). \end{aligned} \quad (45)$$

and

$$\int_{-\infty}^{3/2} \left(-\frac{1}{c} J_z B_\phi \right) 2\pi R \Theta dj = -\frac{1}{4} R_2 B_\phi^2(j=3/2). \quad (46)$$

F. Circuit Model

The electromagnetic force ϵ_{mf} driving the current which implodes the plasma shell is provided by a generator external to the plasma load. The entire system, plasma plus generator or machine, can be modelled by a simple circuit. Let the machine have a constant resistance Z_m and inductance L_m , while the plasma sustains a varying voltage drop V_w at the outer boundary or wall ($r = R_3$). The equation for this circuit is

$$L_m \frac{dI}{dt} + Z_m I = \epsilon_{mf}(t) - V_w(t). \quad (47)$$

To find V_w , integrate Faraday's law, eqn.(9), over the region between the outer plasma radius R_2 and the wall radius R_3 . From relation (14)

$$\frac{D}{Dt} \int_{R(j=2)}^{R(j=3)} B_{\phi} dR - (B_{\phi} V_R)_{j=3} + (B_{\phi} V_R)_{j=2} = cE_Z(R_3) - cE_Z(R_2) .$$

Since $V_R(j=3) = 0$ we have

$$V_w = E_Z(R_3) \Delta Z = \frac{D}{Dt} \int_{R(j=2)}^{R(j=3)} \frac{1}{c} B_{\phi} dR \Delta Z + \Delta Z (B_{\phi} \frac{V_R}{c})_{j=2} + \Delta Z E_Z(R_2) . \quad (48)$$

According to the discussion following eqn.(13), we will ignore the β_{\perp} term in the expression for E_Z from Ohm's law, eqn.(8). The last two terms of the above equation then reduce to $\Delta Z \eta_{\perp}(t) J_Z(j=2, t)$. Since $B_{\phi} = 2I/Rc$ in the outer region [assumption (a-iv) of §II.D] the integral in eqn.(48) can be done explicitly and the time differentiation carried out. The result for the potential drop at the wall is

$$V_w = L_{geo} \frac{dI}{dt} + Z_{geo} I + \eta_{\perp} J_Z(R_2, t) \Delta Z , \quad (49)$$

where

$$L_{geo} \equiv \frac{2}{c^2} \Delta Z \ln \left(\frac{R_3}{R_2} \right) \quad \text{and} \quad Z_{geo} \equiv - \frac{2}{c^2} \Delta Z \frac{V_2}{R_2} \quad (50)$$

are the geometrical inductance and motional resistance arising from the plasma load. Using eqn.(50) in eqn.(47) gives the working equation

$$(L_m + L_{geo}) \frac{dI}{dt} + (Z_m + Z_{geo}) I = \epsilon_{mf} - \eta_{\perp} J_Z(R_2, t) \Delta Z . \quad (51)$$

This equation is solved using a finite difference scheme:

$$\begin{aligned} \left(L_m + L_{geo}^{(n+1/2)} \right) \frac{I^{(n+1)} - I^{(n)}}{\Delta t} + \left(Z_m + Z_{geo}^{(n+1/2)} \right) \frac{I^{(n+1)} + I^{(n)}}{2} \\ = \left[\epsilon_{mf} - \eta_{\perp} J_Z(R_2) \Delta Z \right]^{n+1/2} . \end{aligned} \quad (52)$$

F. Total Energy Conservation.

The plasma plus field total energy equation is the sum of eqns.(12) and (13). The integral of the result from the axis to the outer boundary is the sum of eqns.(20) and (21). If there is no heat flux through the outer wall and eqn.(8) is used for E_z this later sum is

$$\begin{aligned} \frac{D}{Dt} \int_0^{R(j=3)} \left(\rho_i \varepsilon_i + \rho_e \varepsilon_e + \frac{1}{2} \rho_i v_R^2 \right) 2\pi r dr + \frac{D}{Dt} \int_0^{R(j=3)} \left(\frac{B_\phi^2}{8\pi} \right) 2\pi r dr \\ = \frac{1}{\Delta Z} I V_w + \int_0^{R(j=3)} \Lambda 2\pi r dr, \quad (53) \end{aligned}$$

where V_w is the potential drop at the wall according the eqn.(48). Note that $I V_w$ is the input power to the plasma load from the machine while the second term on the right hand side of eqn.(53) is the negative of the radiative loss rate per unit length.

The objective of this section is to derive a corresponding expression for eqn.(53) starting from the difference equations used to advance V , ε_i , ε_e , and v_w , and the differential equation for B_ϕ . Part of this procedure has already been done: the total plasma energy equation was derived in eqn.(30). To derive an energy equation for the field let us start with the expression for the energy input from the machine over the time Δt . From eqn.(49)

$$\begin{aligned} \Delta t \langle I \rangle V_w^{(n+1/2)} = \Delta t \left(\frac{I^{(n+1)} + I^{(n)}}{2} \right) \left[L_{geo}^{(n+1/2)} \frac{I^{(n+1)} - I^{(n)}}{\Delta t} \right. \\ \left. + Z_{geo}^{(n+1/2)} \frac{I^{(n+1)} + I^{(n)}}{2} + \Delta Z \left(\eta_{\perp} J_z(R_2) \right)^{(n+1/2)} \right]. \quad (54) \end{aligned}$$

Using the definitions in eqn.(50), we can rearrange the right hand side of this equation,

$$\left(\frac{I^{(n+1)}}{c} \right)^2 \Delta Z \left[\ln \left(\frac{R_3}{R_2} \right) - \frac{V_2 \Delta t}{2R_2} \right]^{(n+1/2)} - \left(\frac{I^{(n)}}{c} \right)^2 \Delta Z \left[\ln \left(\frac{R_3}{R_2} \right) + \frac{V_2 \Delta t}{2R_2} \right]^{(n+1/2)}$$

$$- \frac{I^{(n+1)} I^{(n)}}{c^2} \Delta Z \left[\frac{V_2 \Delta t}{R_2} \right]^{(n+1/2)} + \langle I \rangle \left[\eta_{\perp} J_Z(R_2) \right]^{(n+1/2)} \Delta Z \Delta t. \quad (55)$$

Note that

$$\begin{aligned} \left[\ln \left(\frac{R_3}{R_2} \right) - \frac{V_2 \Delta t}{2R_2} \right]^{(n+1/2)} &= \ln \left(\frac{R_3}{R_2^{(n+1)}} \right) + \ln \left(\frac{R_2^{(n+1)}}{R_2^{(n+1/2)}} \right) - \frac{V_2^{(n+1/2)} \Delta t}{2R_2^{(n+1/2)}}, \\ &= \ln \left(\frac{R_3}{R_2^{(n+1)}} \right) + \ln \left(\frac{\langle R_2 \rangle}{R_2^{(n+1/2)}} \right) + \ln \left(1 + \frac{\langle V_2 \rangle \Delta t}{2 \langle R_2 \rangle} \right) - \frac{V_2^{(n+1/2)} \Delta t}{2R_2^{(n+1/2)}}. \end{aligned}$$

As long as $|V_2 \Delta t / R_2| \ll 1$, the sum of the last three terms is much less than the first term, which grows as the pinch implodes. A similar expansion can be obtained for the second term in expression (55). Further, we note that for $R_2 < r < R_3$, $B_{\phi} = 2I/rc$, which implies

$$\int_{R(j=2)}^{R(j=3)} \left(\frac{B_{\phi}^2}{8\pi} \right) 2\pi r dr = \frac{I^2}{c^2} \ln \left(\frac{R_3}{R_2} \right).$$

Using the above relations in eqn.(54) gives

$$\begin{aligned} &\left[\int_{R(j=2)}^{R(j=3)} \left(\frac{B_{\phi}^2}{8\pi} \right) 2\pi r dr \right]^{(n+1)} - \left[\int_{R(j=2)}^{R(j=3)} \left(\frac{B_{\phi}^2}{8\pi} \right) 2\pi r dr \right]^{(n)} \\ &= \Delta t \frac{1}{\Delta Z} \langle I \rangle v_w^{(n+1/2)} + \frac{I^{(n+1)} I^{(n)}}{c^2} \frac{V_2^{(n+1/2)} \Delta t}{R_2^{(n+1/2)}} - \Delta t \langle I \rangle \left[\eta_{\perp} J_Z(R_2) \right]^{(n+1/2)}. \quad (56) \end{aligned}$$

We next work on the magnetic field energy in the region $r < R_2$.

$$\left[\int_0^{R(j=2)} \left(\frac{B_{\phi}^2}{8\pi} \right) 2\pi r dr \right]^{(n+1)} - \left[\int_0^{R(j=2)} \left(\frac{B_{\phi}^2}{8\pi} \right) 2\pi r dr \right]^{(n)}$$

$$\begin{aligned}
&= \int_0^2 \frac{1}{4} \left[\left(B_\phi^{(n+1)} \right)^2 R^{(n+1)} \Theta^{(n+1)} - \left(B_\phi^{(n)} \right)^2 R^{(n)} \Theta^{(n)} \right] dj \\
&= \int_0^2 \frac{1}{4} \left[\left(R^{(n+1)} B_\phi^{(n+1)} + R^{(n)} B_\phi^{(n)} \right) \left(\Theta^{(n+1)} B_\phi^{(n+1)} - \Theta^{(n)} B_\phi^{(n)} \right) \right] dj \\
&\quad + \int_0^2 \frac{1}{4} R^{(n+1)} B_\phi^{(n+1)} R^{(n)} B_\phi^{(n)} \left(\frac{\Theta^{(n)}}{R^{(n)}} - \frac{\Theta^{(n+1)}}{R^{(n+1)}} \right) dj . \tag{57}
\end{aligned}$$

For small timesteps

$$\Theta^{(n+1)} B_\phi^{(n+1)} - \Theta^{(n)} B_\phi^{(n)} \approx \Delta t \left(\frac{D}{Dt} (\Theta B_\phi) \right)^{(n+1/2)} = \Delta t \frac{\partial}{\partial j} \left(c \eta_\perp J_Z \right)^{(n+1/2)} ,$$

by eqn.(35), and

$$\frac{\Theta^{(n)}}{R^{(n)}} - \frac{\Theta^{(n+1)}}{R^{(n+1)}} = \frac{\partial}{\partial j} \left[\ln(R^{(n)}) - \ln(R^{(n+1)}) \right] \approx \frac{\partial}{\partial j} \left(- \frac{\langle V \rangle \Delta t}{\langle R \rangle} \right) .$$

Using these last two relations in eqn.(57) and integrating by parts gives

$$\begin{aligned}
&\left[\int_0^{R(j=2)} \left(\frac{B_\phi^2}{8\pi} \right) 2\pi r dr \right]^{(n+1)} - \left[\int_0^{R(j=2)} \left(\frac{B_\phi^2}{8\pi} \right) 2\pi r dr \right]^{(n)} \\
&= \Delta t \frac{1}{4} \left[\left(R_2 B_\phi(R_2) \right)^{(n+1)} + \left(R_2 B_\phi(R_2) \right)^{(n)} \right] c \left[\eta_\perp J_Z(R_2) \right]^{(n+1/2)} \\
&\quad - \Delta t \frac{1}{4} \left(R_2 B_\phi(R_2) \right)^{(n+1)} \left(R_2 B_\phi(R_2) \right)^{(n)} \frac{\langle V_2 \rangle}{\langle R_2 \rangle} \\
&\quad - \Delta t \int_0^{j=2} \frac{1}{2} \left[\left(J_Z R \Theta \right)^{(n+1)} + \left(J_Z R \Theta \right)^{(n)} \right] \left(\eta_\perp J_Z \right)^{(n+1/2)} dj
\end{aligned}$$

$$+ \Delta t \int_0^{R(j=2)} \frac{\langle V \rangle}{c} \frac{1}{2} \left[\left(RB_\phi \right)^{(n+1)} \left(J_Z R \theta \right)^{(n+1)} + \left(RB_\phi \right)^{(n)} \left(J_Z R \theta \right)^{(n+1)} \right] \frac{2\pi}{\langle R \rangle} dj. \quad (58)$$

Finally add eqns.(56) and (58), and note that $B_\phi(R_2) = 2I/R_2c$ to find

$$\begin{aligned} & \frac{1}{\Delta t} \left[\int_0^{R(j=3)} \left(\frac{B_\phi^2}{8\pi} \right) 2\pi r dr \right]^{(n+1)} - \frac{1}{\Delta t} \left[\int_0^{R(j=3)} \left(\frac{B_\phi^2}{8\pi} \right) 2\pi r dr \right]^{(n)} \\ &= \frac{1}{\Delta Z} \langle I \rangle V_w^{(n+1/2)} - \int_0^{R(j=2)} \frac{1}{2} \left[\left(J_Z R \theta \right)^{(n+1)} + \left(J_Z R \theta \right)^{(n)} \right] \left(\eta_\perp J_Z \right)^{(n+1/2)} 2\pi dj \\ &+ \int_0^{j=2} \frac{\langle V \rangle}{c} \frac{1}{2} \left[\left(RB_\phi \right)^{(n+1)} \left(J_Z R \theta \right)^{(n)} + \left(RB_\phi \right)^{(n)} \left(J_Z R \theta \right)^{(n+1)} \right] \frac{2\pi}{\langle R \rangle} dj. \quad (59) \end{aligned}$$

Equation (59) is the derived form of the field energy equation (21). We note that, unlike the derived total energy equation for the plasma [eqn.(30)], eqn.(59) is only valid to first order in Δt . The derived form of the total plasma plus field energy equation is given by the sum of eqns.(30) and (59). Comparison of this result with eqn.(53) indicates the proper time location for the integrand in the resistive heating and $\mathbf{J} \times \mathbf{B}$ work terms, the second and third terms on the right hand side of eqn.(59). However, the required timing of these two terms presents a problem. At step (s-iii) of §II.C for the computation of $V^{(n+1)}$, the quantities $R^{(n+1)}$, $\theta^{(n+1)}$, $B_\phi^{(n+1)}$, and $J_Z^{(n+1)}$ are not known. But we note that to first order in Δt we can make the replacements

$$\frac{1}{2} \left[\left(J_Z R \theta \right)^{(n+1)} + \left(J_Z R \theta \right)^{(n)} \right] \approx J_Z^{(n+1/2)} R^{(n+1/2)} \theta^{(n+1/2)},$$

and

$$\frac{1}{2} \left[\left(RB_\phi \right)^{(n+1)} \left(J_Z R \theta \right)^{(n)} + \left(RB_\phi \right)^{(n)} \left(J_Z R \theta \right)^{(n+1)} \right] \frac{1}{\langle R \rangle} \approx \left(B_\phi J_Z R \theta \right)^{(n+1/2)}.$$

Now the expressions for the resistive heating in eqns.(30) and (59) agree. However, for the $\mathbf{J} \times \mathbf{B}$ work term, $\langle V \rangle$ is inside the integral in eqn.(59), but in eqn.(30) the integral is split up over the j -domain and $\langle V \rangle$ is extracted. In

a full 1-D code there are many zones so that the splitting of the integral is not a severe approximation. In a zero-D code the Maxwell stress term in the momentum equation (23) remains a potential problem for the conservation of total plasma plus field energy. To ameliorate this potential difficulty we have only considered applications of the zero-D code to rapidly collapsing plasmas so that the subsequent rapid resistive heating maintains a narrow skin depth for the current density [see assumption (a-v) of §II.E]. Thus the Maxwell stresses contribute only over a narrow region at the outer boundary of the plasma where $V \approx V_2$. The estimates in eqns.(43)-(46) are to be evaluated as part of the half-step predictor sequence in step (s-ii) of §II.C.

To maintain complete energy conservation $|V_j \Delta t / R_j|$ must be $\ll 1$ as required in the above derivation for field energy conservation. In practice we have found that total energy is conserved to ~2% over an entire simulation with the zero-D code.

III. ATOMIC MODEL AND RADIATION TRANSPORT

The Al atomic model is described in detail by Duston and Davis⁸. There is excited level structure in the eleven highest ionization stages (H-like through Na-like); only ground states are carried for the other stages. For each atomic level included in the model, a rate equation of the form

$$\frac{df_i}{dt} = \sum_j W_{ji} f_j - \sum_j W_{ij} f_i \quad (60)$$

is constructed, where f_i is the fractional population of level i , and W_{ji} is the net reaction rate describing the transition from initial state j to final state i .

For the plasma densities modeled in these studies, the effective populating and depopulating rates are generally fast compared with the hydrodynamic response. An equilibrium assumption can be made in which the explicit time dependence is dropped; in this case, the plasma is said to be in collisional-radiative equilibrium (CRE), wherein the plasma ionization state responds instantaneously to changes in hydrodynamic parameters. The processes included in the transition rates W_{ij} and the methods used in calculating the

corresponding rate coefficients are described elsewhere⁹. Once the rate equations, including radiation transport, have been solved, the electron density and the ionization and excitation energy in the plasma can be calculated.

Radiation emission from a plasma and its opacity are dependent on the local atomic level population densities. Except for optically thin plasmas, however, these populations also depend on the radiation field through optical pumping, photoionization and photoexcitation. Thus, the atomic physics processes and radiation transport are strongly coupled and must be solved self-consistently. In this model, an iterative procedure¹⁰ is used in which the radiation field from the previous iteration is used to solve for new f_i , from which a new radiation field is calculated and populations are recalculated until convergence is achieved.

A hybrid model is used to transport the radiation. Free-free radiation is treated on a multifrequency basis. The line and bound-free radiation is transported via a probabilistic model¹¹.

IV. AVERAGE-ATOM MODEL

A time-dependent average atom model has been developed which solves hydrogenic rate equations for a set of orbital population levels P_n , where $1 \leq n \leq 10$. These rate equations are nonlinear and are of the form

$$\frac{dP_n}{dt} = -P_n \sum_m D(n \rightarrow m) Q_m + Q_n \sum_m C(m \rightarrow n) P_m - P_n I_n + Q_n R_n, \quad (61)$$

where $Q_n = (1 - P_n/g_n)$, I_n is the ionization rate of level n , R_n is the recombination rate into level n , $D(n \rightarrow m)$ is the destruction rate of level n by transition to level m , $C(m \rightarrow n)$ is the creation rate of level n by transition from level m , and g_n is the degeneracy of level n and is given by $2n^2$ for hydrogenic levels. The model includes radiative and three-body recombination, collisional excitation and de-excitation and radiative decay in the rates. This model is based largely on the work of Post, et. al.¹².

Once the populations P_n have been calculated, the average charge and radiative cooling rate can be determined. An approximate way of generating n_l

subshell populations and energies has been devised; in this way, $\Delta n=0$ transitions can be treated. This treatment of $\Delta n=0$ transitions differs from the more complicated approach of Post, et. al. Bremsstrahlung, bound-free, and line radiation are included in the radiative cooling.

The rates in the Al atomic model used in these studies were not considered reliable for electron temperatures below about 20 eV, so the average-atom model was sometimes used for electron temperature lower than this.

V. APPLICATION TO ALUMINUM VAPORS

A. Plasma Shells of Varying Thickness

The ZPIMP code described in the above sections was used to simulate the implosion of aluminum plasma shells of varying mass loading and initial radii. Mass loadings of 30, 35, and 40 $\mu\text{g}/\text{cm}$ were considered. Initial outer and inner radii pairs were (1.00, 0.90), (1.05, 0.85), and (1.15, 0.75) cm; these pairings gave initial shell thickness of 0.1, 0.2, and 0.4 cm. Initial electron and ion temperatures of 5eV were assumed. The coefficient of the artificial viscosity, b_{vis} , was set at 0.25 after comparison of some test runs with a multi-zone 1-D Lagrangian code. The resistivity is given by Braginskii's⁶ form in the high field limit. For the machine inductance we used $L_m = 58$ nanohenrys; for the machine impedance $Z_m = 2$ Ohms; and the open circuit voltage was chosen to match GAMBLE II.

Figure 1 shows the minimum outer radius $R_{2,\text{min}} = \min\{R_2(t)\}$ obtained in this series of runs (the minimum inner radius always went to zero). The smallest of the $R_{2,\text{min}}$ always occurs for the lowest mass loadings and thinnest shells. Figure 2 gives the times of peak compression for this set of calculations. The earliest compression times again occur for the lowest mass loadings and thinnest shells.

This pattern of the extremum occurring for the lowest mass loadings and thinnest shells also occurs in the next several plots (Figs. 3-7) for electron temperature, average charge and radiated power. The higher radiative cooling under these conditions allows the plasma to be compressed to higher densities

(or smaller radii). The exceptions are the line and continuum radiation maxima below the K edge, which are fairly flat.

All the \bar{Z} maxima are well above 11, which means that the Al ions are usually in the He-like and H-like states at peak compression. This is reflected in the fact that the line and continuum radiation maxima above the K edge are higher than those below the K edge. These results indicate that, under the set of conditions simulated by these calculations, it should be possible to create highly-ionized Z-pinch Al plasmas in the NRL GAMBLE II device.

B. Filled Cylinder Plasmas

Using the same mass loadings, a set of filled-shell (inner radius=0) runs were made for different initial outer radii ranging from 0.5 cm to 2.0 cm. Initial temperatures of 5eV were assumed. The next several figures show some results from these calculations.

Figure 8 shows the minimum outer radius $R_{2,\min}$ obtained at each mass loading vs. initial outer radius $R_{2,o}$. Generally, the trend is for $R_{2,\min}$ to increase with $R_{2,o}$. However, the 35 $\mu\text{g}/\text{cm}$ curve peaks slightly at $R_{2,o}=1.875$ cm, and the 40 $\mu\text{g}/\text{cm}$ curve shows a very pronounced dip between 1.625 cm and 2.0 cm. Unlike Figure 1, the smaller $R_{2,\min}$ occurs at the larger mass loadings.

Figure 9 gives the times of maximum implosion ($R_2 = R_{2,\min}$) vs. $R_{2,o}$ for the different mass loadings. The larger times occur at the larger mass loading and larger $R_{2,o}$, generally.

Figure 10 displays the maximum electron temperatures achieved during these calculations. These maxima usually occurred at, or just prior to, maximum implosion. The higher maximum temperatures result at the lower masses. The 40 $\mu\text{g}/\text{cm}$ curve drops very rapidly in the area where $R_{2,\min}$ also decreases rapidly, then it seems to stabilize as $R_{2,\min}$ increases again.

The maximum average ionic charge \bar{Z} is shown in Figure 11. The results seem to peak around $R_{2,o}=1.0$; the highest ionization occurs at the smallest mass. The 40 $\mu\text{g}/\text{cm}$ curve crosses $\bar{Z}=11$ in the region where $R_{2,\min}$ drops rapidly. When \bar{Z} is 11 or greater, He-like and H-like ions are predominant. When \bar{Z} drops below 11, L-shell radiation appears. The result of \bar{Z} falling

below 11 is enhanced L-shell and total radiation as will be seen in subsequent figures.

Figure 12 shows the maximum total radiated power for these runs. The higher radiation occurs for the larger mass, which helps to explain the fact that the smaller $R_{2,\min}$ occur with the larger mass.

Figures 13 and 14 give the maximum line and continuum radiation below and above the K edge. Figures 12, 13a, and 14a show an increase in radiated power at 40 $\mu\text{g}/\text{cm}$ at $R_{2,0} \approx 1.69$ cm. This is the point at which maximum \bar{Z} crosses 11 and at which $R_{2,\min}$ decreases rapidly. The enhanced cooling of the plasma, as shown in Figure 10, reduces plasma pressure and allows for increased compression. Beyond $R_{2,0} \approx 1.75$ cm, the radiative cooling drops; plasma thermal energy is retained and it becomes harder to compress the plasma. Hence $R_{2,\min}$ increases again.

It should also be noted in Figures 13a and 14a that the L-shell radiative cooling reaches a minimum at large $R_{2,0}$ and rises again for the 35 $\mu\text{g}/\text{cm}$ mass. This accounts for the peak in this $R_{2,\min}$ curve noted earlier.

These curves show high radiative losses at low $R_{2,0}$ for all the mass loadings; hence, all $R_{2,\min}$ are small at small $R_{2,0}$.

VI. SUMMARY

The equations and structure of the new, zero-D, ZPIMP code have been presented. This code combines the best features of previous, but separate, zero-D codes, such as the coupling of a CRE ionization model with radiation transport in SIMPLODE³, and a self-consistent circuit equation as in McDonald and Ottinger's⁵ code. However, ZPIMP uses a completely different approach for the hydrodynamics: the continuity, momentum, and energy equations are solved in a finite difference form similar to a standard multi-zone Lagrangian code. Furthermore, rather than specifying a profile for the current density, ZPIMP uses an analytic solution to the induction equation for the diffusion of the magnetic field in a moving medium. The form of the total (plasma + field) energy conservation relation is explicitly derived from the finite difference equations.

The detailed development of the equations in the text clarifies the inherent limitations of a zero-D model for an imploding plasma. Besides the

oversimplification of an average value for the plasma density and temperature, the bounce phase of an imploding annular shell is poorly handled. Pressure forces in the plasma between the shell and the axis are always ignored in a zero-D code, but do become significant at the time of bounce. Within the framework of the ZPIMP code this problem could readily be corrected by solving the dynamics over the inner zone, as well as the plasma shell. Since the mass in the inner zone is much less than that in the shell zone, one could still restrict the time consuming radiation transport to the main plasma shell. For the existing ZPIMP code, the results for general trends at the collapse time are consistent with several runs made with multi-zone codes. The ZPIMP simulation is also limited to rapid collapse times since the gradient scale length of the magnetic field was assumed to be small compared to the plasma radius. This condition allowed a simple solution to the induction equation for annular shells. Future improvements to the hydrodynamics and magnetic diffusion in ZPIMP are under development.

The zero-D ZPIMP code has been applied to the implosions of an aluminum vapor in annular shells and filled cylinders. The parameters of the circuit were chosen to match the NRL GAMBLE II device. The effects of various mass loadings, initial outer radii, and shell widths on the gross properties of the implosion were discussed. In particular, results for the implosion time and radius, maximum charge state and temperature, and peak radiated power have been summarized in the figures. In a future report we will analyze the radiative yields, spectra, and pulse durations as a function of the mass loading and initial configuration of the aluminum vapor. This large parameter space can only be effectively studied with a versatile and rapid zero-D code such as ZPIMP. From a comparison of the results we intend to determine the optimum conditions for aluminum K- and L-shell radiation.

ACKNOWLEDGEMENTS

We gratefully acknowledge several fruitful discussions with J. Davis, R. Terry, and V. Thornhill during the course of this work. The research was sponsored by the Defence Nuclear Agency under Subtask Code and Title: RL RA/Advanced Simulation Concepts, Work Unit Code & Title, 00050, X-Ray Source Development Theory, and by the Office of Naval Research.

REFERENCES

- ¹J. Stephanakis, S. W. McDonald, R. A. Meger, P. F. Ottinger, F. C. Young, C. G. Mehlman, J. P. Apruzese, and R. E. Terry, Bull. Amer. Phys. Soc., **29**, 1232 (1984); J. Stephanakis, J. P. Apruzese, P. G. Burkhalter, J. Davis, R. A. Meger, S. W. McDonald, C. G. Mehlman, P. F. Ottinger, and F. C. Young, Appl. Phys. Lett., **48**, 829 (1986).
- ²J. U. Guillory and R. E. Terry, Defanse Nuclear Agency Report, #6304F, (1984).
- ³J. Davis, C. Agritellis, and D. Duston, NRL Memorandum, 5615, (1985).
- ⁴J. Davis, J. E. Rogerson, and J. P. Apruzese, NRL Memorandum, 5776, (1986); J. Davis, J. E. Rogerson, and J. P. Apruzese, NRL Memorandum, 5765, (1986).
- ⁵S. W. McDonald and P. F. Ottinger, NRL Memorandum, 5785, (1986).
- ⁶S. I. Braginskii, "Transport Processes in a Plasma", in Reviews of Plasma Physics, Vol. I, ed. M. A. Leontovich, (Consultants Bureau: New York, 1965), p. 205.
- ⁷E. M. Epperlein and M. G. Haines, "Plasma Transport Coefficients in a Magnetic Field by Direct Numerical Solution of the Fokker-Planck Equation", Phys. Fluids, **29**, 1029 (1986).
- ⁸D. Duston and J. Davis, Phys. Rev. A, **23**, 2602, (1981).
- ⁹D. Duston, R. W. Clark, J. Davis, and J. P. Apruzese, Phys. Rev. A, **27**, 1441 (1983).

- ¹⁰J. P. Apruzese, J. Davis, D. Duston, and R. W. Clark, Phys. Rev. A, 29, 246 (1984).
- ¹¹J. P. Apruzese, J. Davis, D. Duston, and K. G. Whitney, JQSRT, 23, 475 (1980); J. P. Apruzese, JQSRT, 25, 419 (1981).
- ¹²D. E. Post, R. V. Jensen, C. B. Tarter, W. H. Grasberger, and W. A. Lokke, Atomic Data and Nuclear Data Tables, 20, 397 (1977).

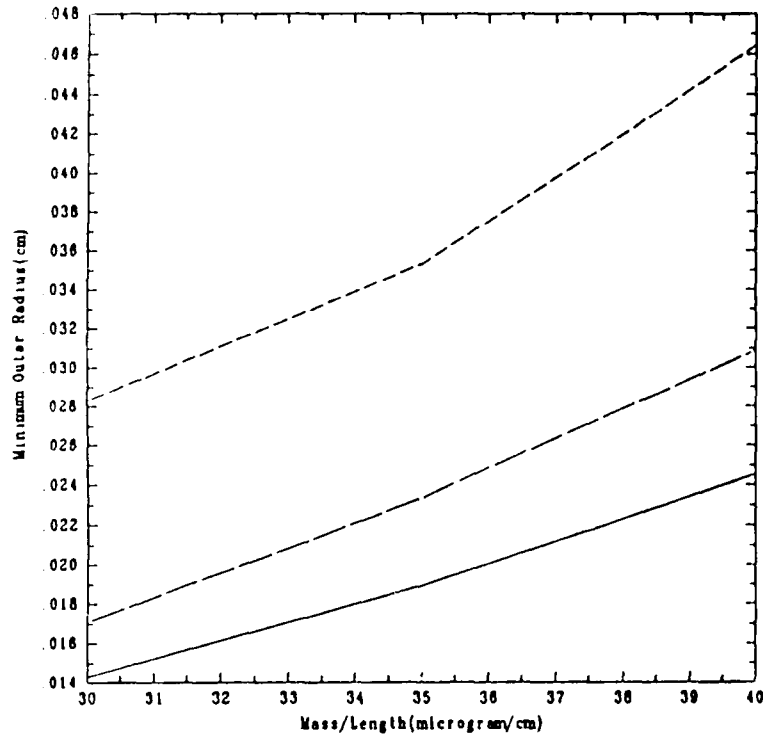


Fig 1. Minimum outer radius for the thin shell Al plasma implosions. The solid line represents a shell thickness $\Delta R = 0.1$ cm, the long dashed line represents $\Delta R = 0.2$ cm, and the short-dashed line represents $\Delta R = 0.4$ cm.

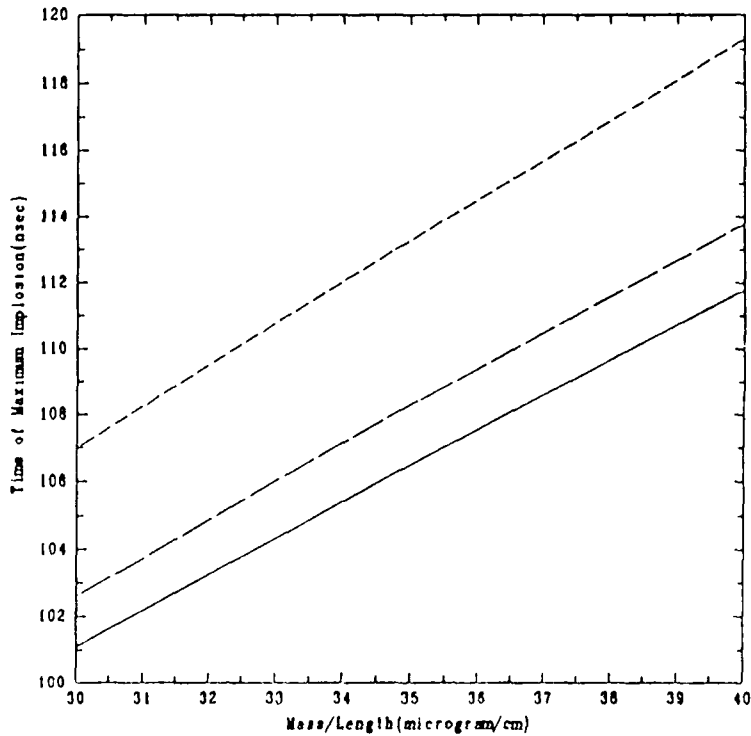


Fig 2. Time of maximum implosion for the thin shell cases. Same notation as Figure 1.

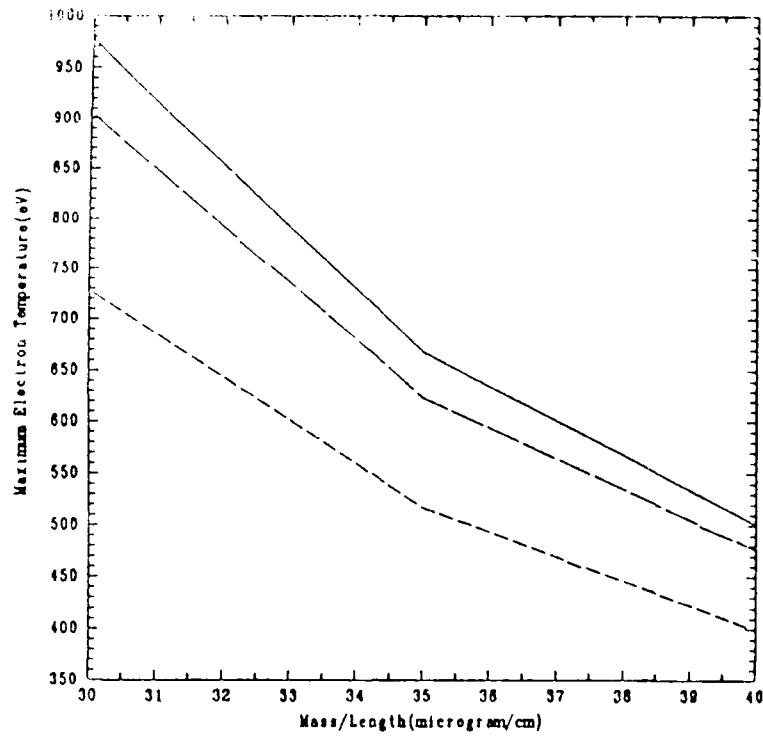


Fig 3. Maximum electron temperature for the thin shell cases. Same notation as Figure 2.

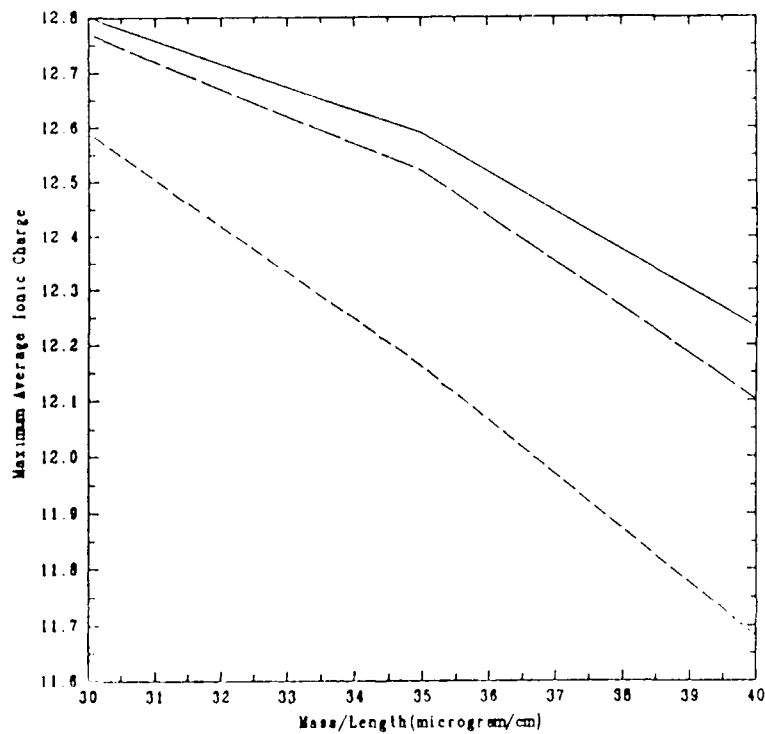


Fig 4. Maximum average ionic charge for the thin shell cases. Same notation as Figure 1.

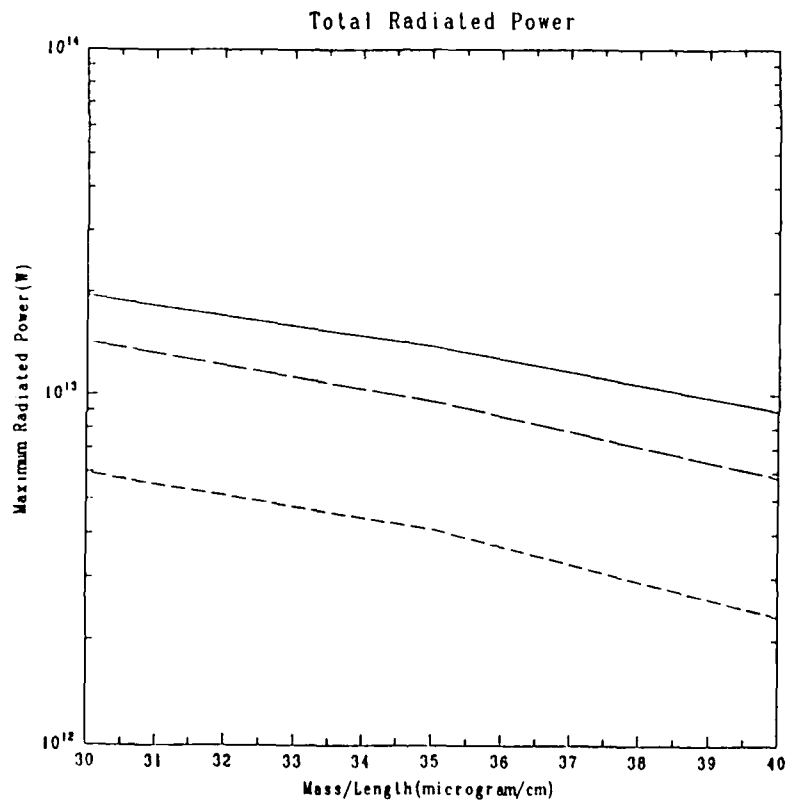


Fig 5. Maximum total radiated power for the thin shell cases. Same notation as Figure 1.

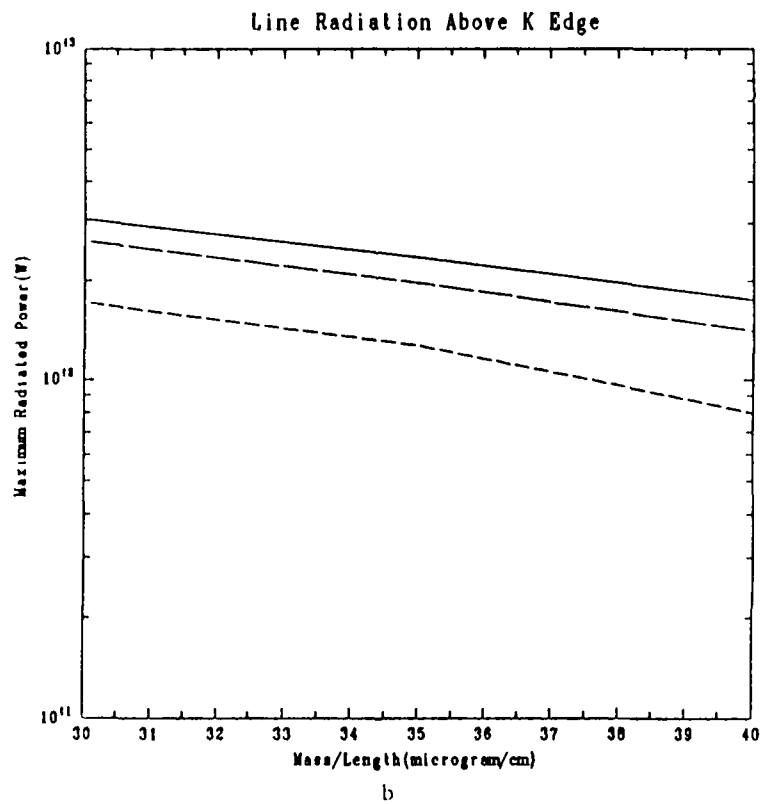
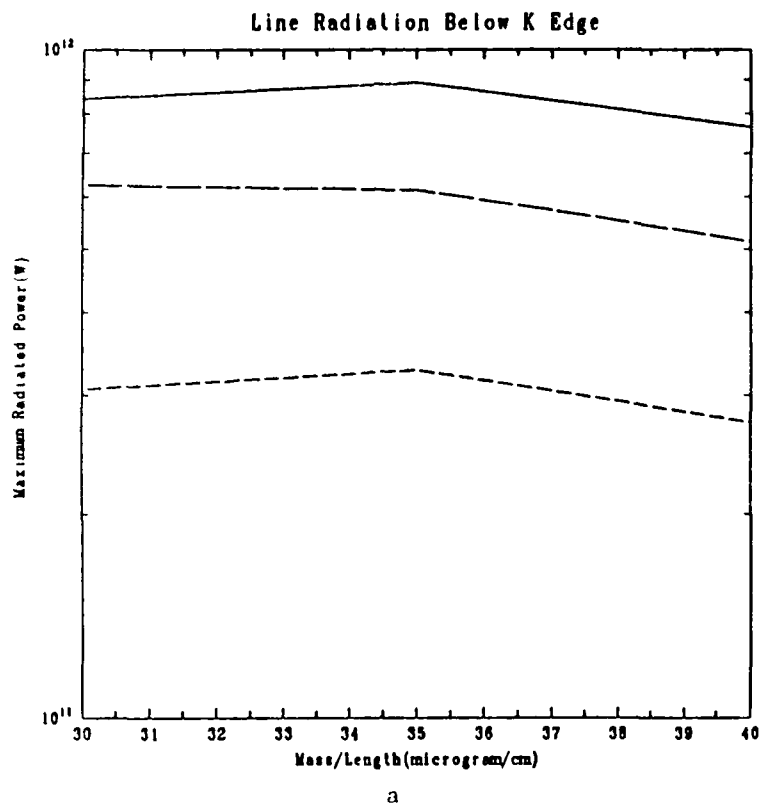
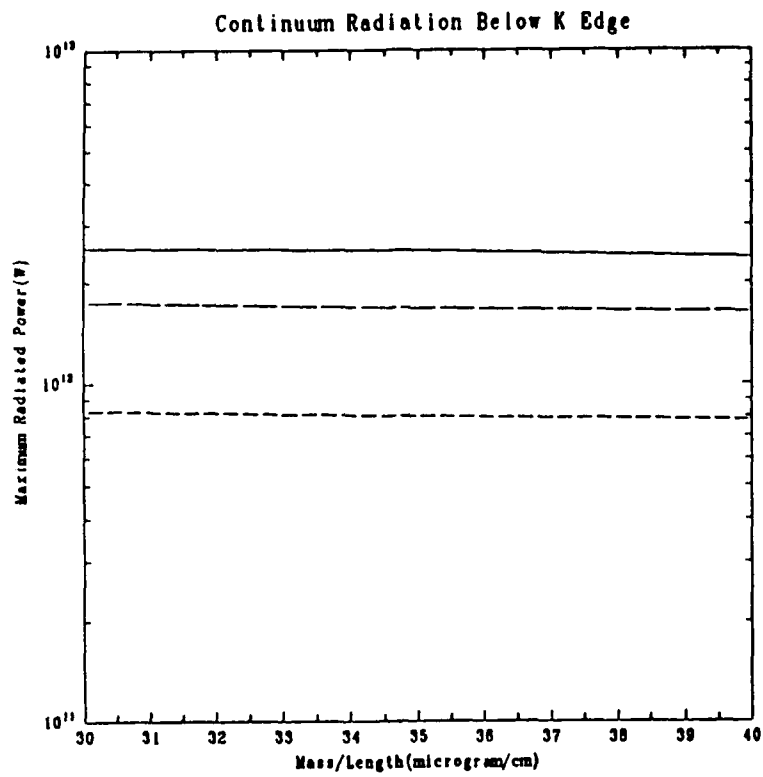
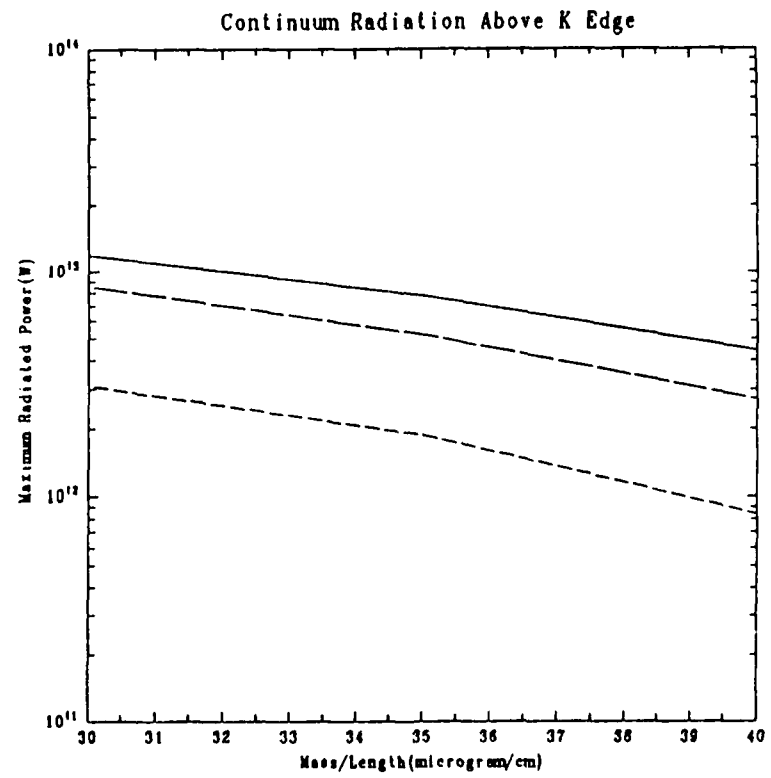


Fig 6. Maximum line radiation below (a) and above (b) the K edge for the thin shell cases. Same notation as Figure 1.



a



b

Fig 7. Maximum continuum radiation below (a) and above (b) the K edge for the thin shell cases. Same notation as Figure 1.

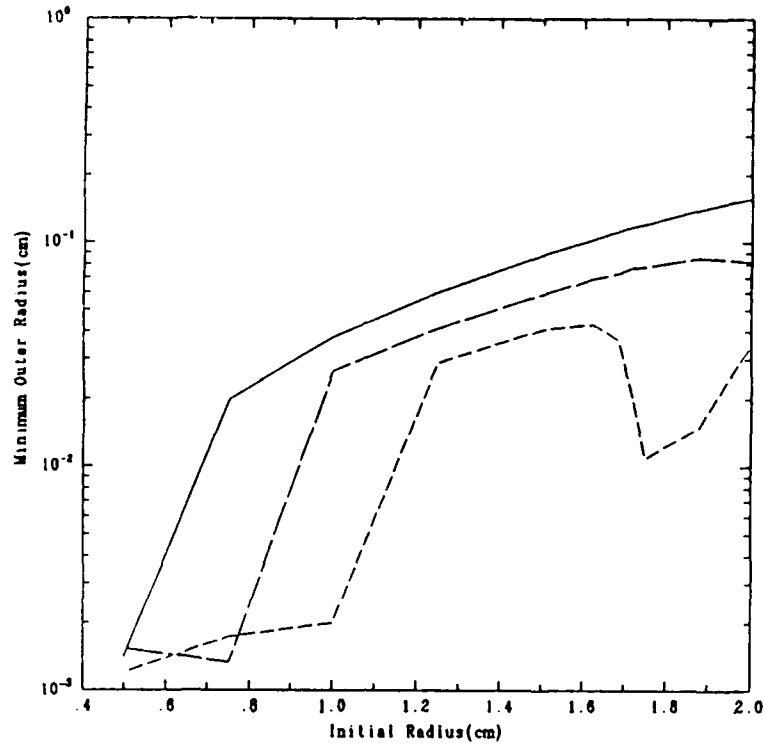


Fig 8. Minimum outer radius for the filled cylinder Al plasma implosions. The solid line is 30 $\mu\text{g}/\text{cm}$, the long-dashed line is 35 $\mu\text{g}/\text{cm}$, and the short-dashed line is 40 $\mu\text{g}/\text{cm}$.

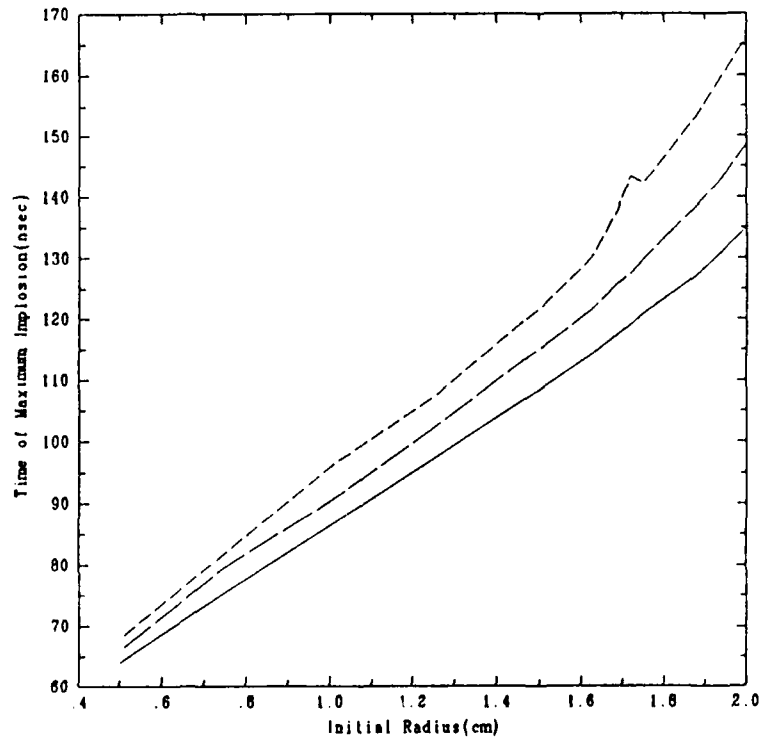


Fig 9. Time of maximum implosion for the filled cylinder cases. Same notation as Figure 8.

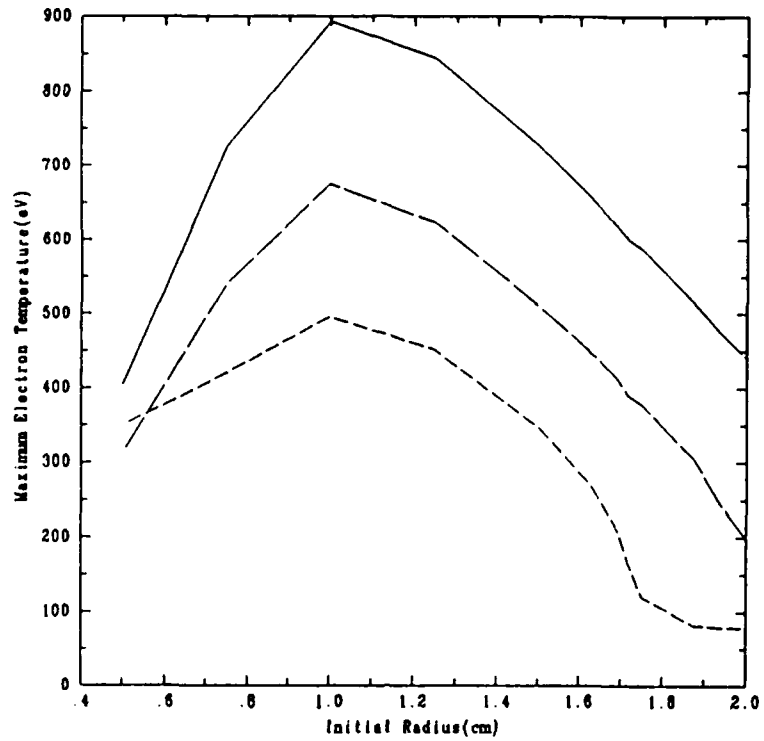


Fig 10. Maximum electron temperature for the filled cylinder cases.
Same notation as Figure 8.

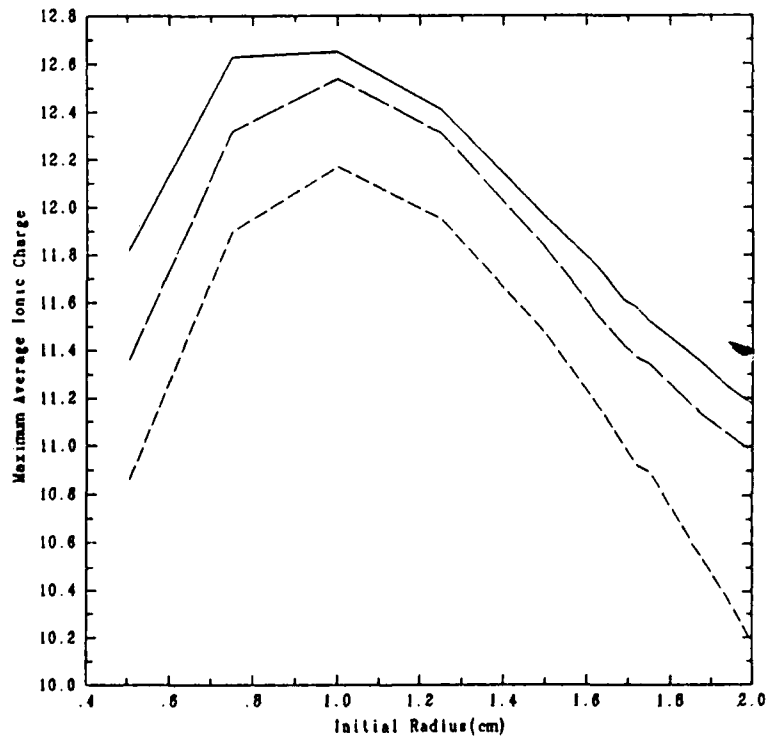


Fig 11. Maximum average ionic charge for the filled cylinder cases.
Same notation as Figure 8.

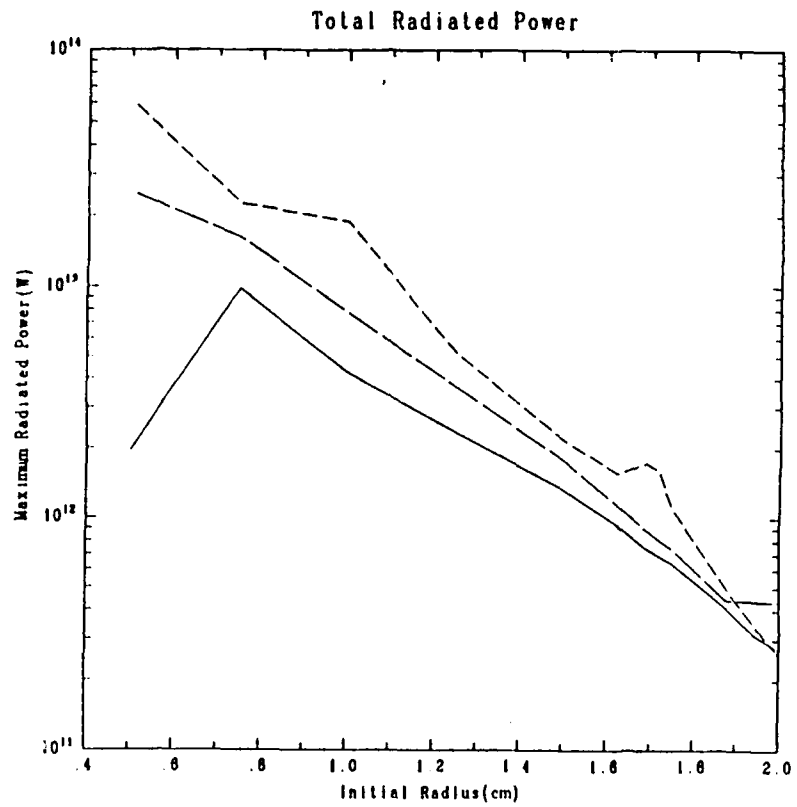


Fig 12. Maximum total radiated power for the filled cylinder cases. Same notation as Figure 8.

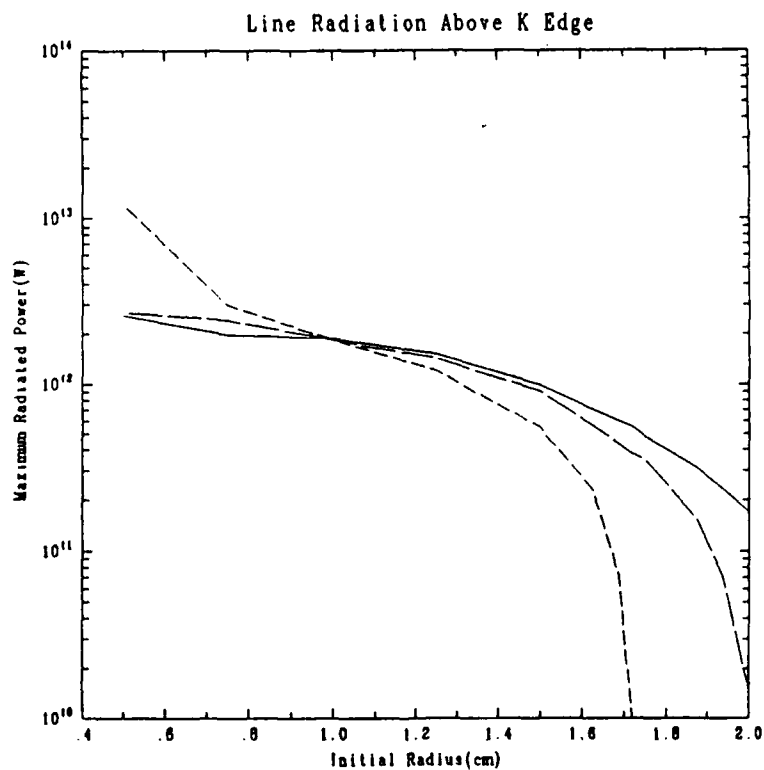
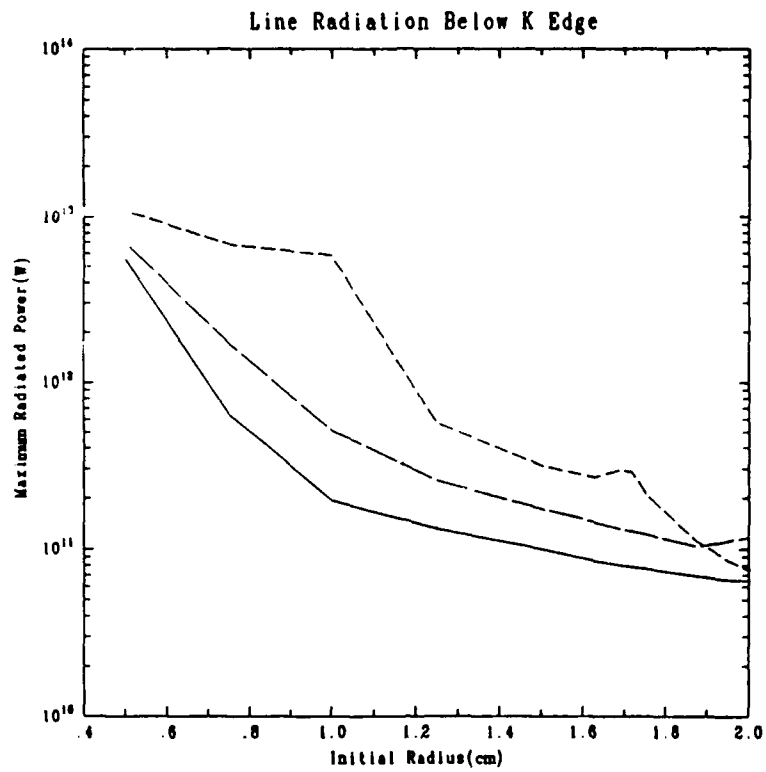


Fig 13. Maximum line radiation below (a) and above (b) the K edge for the filled cylinder cases. Same notation as Figure 8.

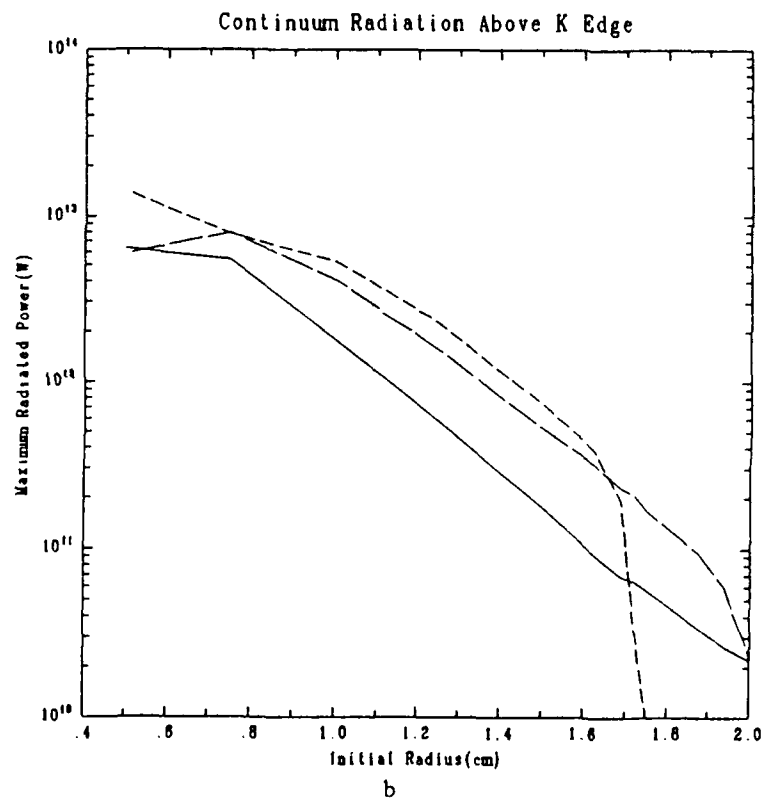
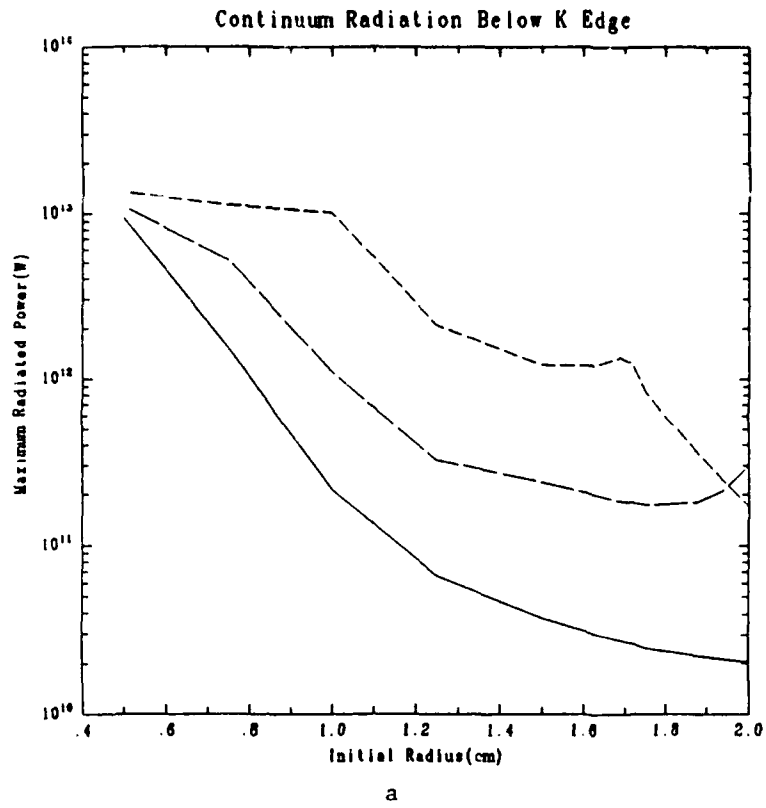


Fig 14. Maximum continuum radiation below (a) and above (b) the K edge for the filled cylinder cases. Same notation as Figure 8.

DISTRIBUTION LIST

| | |
|---|--|
| Assistant to the Secretary of Defense Atomic Energy Washington, D.C. 20301 Attn: Executive Assistant | 1 copy |
| Director Defense Nuclear Agency Washington, D.C. 20305 Attn: DDST TITL RAEV STVI | 1 copy 4 copies 1 copy 1 copy |
| Commander Field Command Defense Nuclear Agency Kirtland AFB, New Mexico 87115 Attn: FCPR | 1 copy |
| Chief Field Command, Livermore Division Department of Defense Post Office Box 808 Livermore, California 94550 Attn: FCPRL | 1 copy |
| Director Joint Strat TGT Planning Staff Offutt AFB Omaha, Nebraska 68113 Attn: JLKS | 1 copy |
| Undersecretary of Defense for RSCH and ENGRG Department of Defense Washington, D.C. 20301 Attn: Strategic and Space Systems (OS) | 1 copy |
| Deputy Chief of Staff for RSCH DEV and ACQ Department of the Army Washington, D.C. 20301 Attn: DAMA-CSS-N | 1 copy |
| Commander Harry Diamond Laboratories Department of the Army 2800 Powder Mill Road Adelphi, Maryland 20783 Attn: DELHD-N-NP DELHD-R J. Rosado DELHD-TA-L (Tech. Lib.) | 1 copy each |

| | |
|---|--------------------|
| U.S. Army Missile Command Redstone Scientific Information Center Attn: DRSMI-RPRD(Documents) Redstone Arsenal, Alabama 35809 | 3 copies |
| Commander U.S. Army Nuclear and Chemical Agency 7500 Backlick Road Building 2073 Springfield, Virginia 22150 Attn: Library | 1 copy |
| Commander Naval Intelligence Support Center 4301 Suitland Road, Bldg. 5 Washington, D.C. 20390 Attn: NISC-45 | 1 copy |
| Commander Naval Weapons Center China Lake, California 93555 Attn: Code 233 (Tech. Lib.) | 1 copy |
| Officer in Charge White Oak Laboratory Naval Surface Weapons Center Silver Spring, Maryland 20910 Attn: Code R40 Code F31 | 1 copy each |
| Air Force Weapons Laboratory Kirtland AFB, New Mexico 87117 Attn: SUL CA | 1 copy each |
| Deputy Chief of Staff Research, Development and Accounting Department of the Air Force Washington, D.C. 20330 Attn: AFRDQSM | 1 copy |
| Commander U.S. Army Test and Evaluation Command Aberdeen Proving Ground, Maryland 21005 Attn: DRSTE-EL | 1 copy |

| | |
|---|-------------|
| Auburn University Department of Physics Attn: Dr. J. Perez Auburn, Al 36849 | 1 copy |
| AVCO Research and Systems Group 201 Lowell Street Wilmington, Massachusetts 01887 Attn: Library A830 | 1 copy |
| BDM Corporation 7915 Jones Branch Drive McLean, Virginia 22101 Attn: Corporate Library | 1 copy |
| Berkeley Research Associates Post Office Box 983 Berkeley, California 94701 Attn: Dr. Joseph Workman | 1 copy |
| Berkeley Research Associates Post Office Box 852 5532 Hempstead Way Springfield, Virginia 22151 Attn: Dr. Joseph Orens | 1 copy each |
| Boeing Company Post Office Box 3707 Seattle, Washington 98134 Attn: Aerospace Library | 1 Copy |
| The Dikewood Corporation 1613 University Blvd., N.E. Albuquerque, New Mexico 87110 Attn: L. Wayne Davis | 1 copy |
| General Electric Company - Tempo Center for Advanced Studies 816 State Street Post Office Drawer QQ Santa Barbara, California 93102 Attn: DASIAC | 1 Copy |
| Institute for Defense Analyses 1801 N. Beauregard Street Alexandria, Virginia 22311 Attn: Classified Library | 1 copy |
| IRT Corporation Post Office Box 81087 San Diego, California 92138 Attn: R. Mertz | 1 copy |

| | |
|---|-------------|
| JAYCOR 1608 Spring Hill Road Vienna, Virginia 22180 Attn: R. Sullivan | 1 copy |
| JAYCOR 11011 Forreyane Road Post Office Box 85154 San Diego, California 92138 Attn: E. Wenaas F. Felbar | 1 copy |
| KAMAN Sciences Corporation Post Office Box 7463 Colorado Springs, Colorado 80933 Attn: Library | 1 copy each |
| Lawrence Livermore National Laboratory University of California Post Office Box 808 Livermore, California 94550 Attn: DOC CDN for 94550 DOC DCN for L-47 L. Wouters DOC CDN for Tech. Infor. Dept. Lib. | 1 copy each |
| Lockheed Missiles and Space Company, Inc. Post Office Box 504 Sunnyvale, California 94086 Attn: S. Taimlty J.D. Weisner | 1 copy each |
| Maxwell Laboratory, Inc. 9244 Balboa Avenue San Diego, California 92123 Attn: A. Kolb M. Montgomery J. Shannon K. Ware | 1 copy ea. |
| McDonnell Douglas Corporation 5301 Bolsa Avenue Huntington Beach, California 92647 Attn: S. Schneider | 1 copy |
| Mission Research Corporation Post Office Drawer 719 Santa Barbara, California 93102 Attn: C. Longmire | 1 copy each |
| Mission Research Corporation-San Diego 5434 Ruffin Road San Diego, California 92123 Attn: Victor J. Van Lint | 1 copy |

| | |
|---|-------------|
| Northrop Corporation Northrop Research & Technology Center 1 Research Park Palos Verdes Peninsula, California 90274 | 1 copy |
| Physics International Company 2700 Merced Street San Leandro, California 94577 Attn: M. Krishnan C. Gilman S. Wong | 1 copy |
| R and D Associates Post Office Box 9695 Marina Del Rey, California 90291 Attn: Library | 1 copy each |
| Sandia National Laboratories Post Office Box 5800 Albuquerque, New Mexico 87115 Attn: Doc Con For 3141 D. McDaniel P. VanDevender K. Matzen, Code 4247 | 1 copy each |
| Science Applications, Inc. Post Office Box 2351 La Jolla, California 92038 Attn: R. Beyster | 1 copy |
| Spectra Technol, Inc., 2755 Northup Way Bellevue, Washington 98004 Attn: Alan Hoffman | 1 copy |
| Spire Corporation Post Office Box D Bedford, Massachusetts 07130 Attn: R. Little | 1 copy |
| S-CUBED Post Office Box 1620 La Jolla, California 92038 Attn: A. Wilson | 1 copy |
| Director Strategic Defense Initiative Organization Pentagon 20301-7100 Attn: DE Lt. Col Richard Gullickson/DEO IST Dr. Dwight Duston IST Dr. Jonathan Farber | 1 copy each |

Texas Tech University
Post Office Box 5404
North College Station
Lubbock, Texas 79417
Attn: T. Simpson

1 copy

TRW Defense and Space Systems Group
One Space Park
Redondo Beach, California 90278
Attn: Technical Information Center

1 copy

Naval Research Laboratory
Plasma Radiation Branch
Washington, D.C. 20375
Code 4720 - 50 copies
4700 - 26 copies
2628 - 22 copies